TIME SERIES ANALYSIS FOR THE CF SOURCE IN SUDBURY NEUTRINO OBSERVATORY

A Thesis

Presented to

The Faculty of Graduate Studies

of

The University of Guelph

by

HENDRICK LABRANCHE

In partial fulfilment of requirements

for the degree of

Master of Science

September, 2003

ABSTRACT

TIME SERIES ANALYSIS FOR THE CF SOURCE IN SUDBURY NEUTRINO OBSERVATORY

Hendrick Labranche
University of Guelph, 2003

Advisor:
Professor Jimmy Law

The Sudbury Neutrino Observatory uses a ^{252}Cf source to measure the neutron detection efficiency of its detector. We propose a method, the Time Series Analysis, that uses pairs of time intervals between the detected events to find the neutron detection efficiency, the probability to detect from a fission the prompt γ-rays, the neutron mean life inside the detector, the source fission rate and the residual activity rate from non-fission events. We explain our theoretical model of the source and the procedure to fit the data. With a 2.5 MeV threshold cut on the data, the neutron mean life is 5.281$\pm$0.004(stat) msec and the source fission rate at June 12, 2001 is 4.360$\pm$0.004(stat) sec^{-1}. At this moment, the Time Series can only be applied to data when the source is near the centre. The technique is also applied with an AmBe source. We also show the latest progress to improve the technique. Finally, we briefly show another method, the Multiplicity Analysis, which was used before we changed to the Time Series.

Acknowledgments

I would like first to thank Prof. Bernie G. Nickel. He spent his time on this project with so much generosity, particularly to have conceived the whole Time Series theoretical model and for his patient times to explain me the details of that model. The developement of a new method of analysis through a multitude of physical concepts was really great to do. I thank my supervisor Prof. Jimmy Law for his help and his support. Also, I thank Dr Ian Lawson, for his generous help to demystify computers, he saves me a lot of time through many technical problems. I do not forget Professor John Simpson, Dr P. Jagam and several SNO's members who teached me a lot of things through the SNO project.

J'en profite aussi pour dire un salut à Marc, Vincent, David et Sylvie avec qui j'ai eu un beaucoup de plaisir à étudier la physique au baccalauréat. Je leur doit en parti ma réussite et mon goût pour cette science.

Contents

List of Tables

List of Figures

Chapter 1

Introduction

Over the past 30 years, solar neutrino experiments have measured fewer electron-neutrinos reaching the Earth than expected by models of the Sun [1, 2]. These models predict electron-neutrino emissions from the thermonuclear reactions in the centre of the Sun. Since the previous experiments are sensitive to only electron-neutrinos, one promising explanation of this neutrino flux deficit is the transformation of the Sun's electron-neutrinos into other flavours. This hypothesis called for new experiments which were able to detect efficiently all neutrino flavours, and the Sudbury Neutrino Observatory was built to make this measurement.

1.1 The Sudbury Neutrino Observatory

The Sudbury Neutrino Observatory (SNO) is a large volume heavy water detector which has the potential to measure both the electron-neutrino (ν_e) flux from the Sun and the total solar neutrino flux (ν_e, ν_μ and ν_τ) independent of neutrino type. With this detector it is possible to test models of solar energy generation and, independently, to search for neutrino oscillations with great sensitivity.

The detector is located in a cavern more than 2000 meters below ground in the Creighton Mine, in the city of Greater Sudbury, Ontario. It uses 1000 metric tons of ultrapure D_2O in a 12 m diameter spherical acrylic vessel. This sphere is surrounded by ultrapure H_2O. A stainless steel structure 17.8 m in diameter supports 9456 20-cm photomultiplier tubes.

SNO measures the ^8B solar neutrinos through these reactions in the D_2O:

$$\begin{aligned} \nu_e + d &\longrightarrow \quad p + p + e^- \quad (CC) \\ \nu_x + d &\longrightarrow \quad \nu_x + p + n \quad (NC) \\ \nu_x + e^- &\longrightarrow \quad \nu_x + e^- \quad (ES) \end{aligned}$$

The charged current reaction is sensitive exclusively to electron-neutrinos, while the neutral current (NC) and the elastic scattering (ES) reactions are sensitive to all three flavours ($x = e, \mu, \tau$). The charged current and the elastic scattering reactions are detected by the electron Čerenkov radiation. The neutral current reaction is detected from the neutron capture by a nucleus in the heavy water.

The main purpose of this thesis is to develop a new method to determine the neutron capture detection efficiency of the SNO detector.

1.2 The Neutron Capture Detection Efficiency

From November 1999 to May 2001, SNO completed Phase I of the experiment, which recorded events in ultrapure D_2O. The results from Phase I were published in 2001 [3] and 2002 [4], presenting the first estimate of the neutrino fluxes in pure D_2O. Whereas the CC reaction rate was high enough to provide good statistics in Phase I, the NC reaction was much lower. After 306.4 live days, with a kinetic energy threshold cut of

5 MeV and a fiducial volume cut at 550 cm from detector centre, the results were [4]

$$\begin{aligned} CC\ events &= 1967.7^{+61.9}_{-60.9}(stat) \\ NC\ events &= 576.5^{+49.5}_{-48.9}(stat). \end{aligned}$$

Since May 2001, a small concentration of NaCl was mixed with the heavy water as SNO's Phase II experiment. The effect of NaCl is to increase the neutron capture detection efficiency as the ^{35}Cl has a very high neutron capture cross section. Since SNO expects a higher NC contribution during Phase II than Phase I, the need of accuracy for the neutron detection efficiency becomes more important.

To find this efficiency, a californium (Cf) neutron source was made and put inside the acrylic vessel (AV). The neutrons emitted by the source can then be recorded by the detector and analysed to get an efficiency value. By moving the source to different positions inside the AV, we get an efficiency as a function of the radial position of the source. Since the beginning of the SNO Salt Phase (Phase II), two methods have been used by Kos [5] to find the neutron detection efficiency, called the Burst Analysis Method and the Direct Counting Method. Because these two methods are directly dependent on a measurement of the Cf source strength, it would be very helpful if an new method that is independent of the source strength measurement can be developed.

During the pure D_2O Phase (Phase I), the Multiplicity Analysis [6, 7] was used as a source strength independent method to extract the detection efficiency. While this method was an efficient technique in the pure D_2O Phase, the new physical situation provided by the Salt Phase and the need for greater accuracy makes the Multiplicity Method inadequate (this method will be discussed later). Based on the characteristics of the source isotopes, a new method to analyse the Cf source data

has been developed. We call this method the Time Series Analysis.

1.3 The Time Series Analysis

The Time Series Analysis is built from the intrinsic characteristics of the ^{250}Cf and the ^{252}Cf fissions, which are the main neutron emitters from SNO's Cf source. From these characteristics, a probabilistic function, called the survival function, was developed to show what the chronology of the intervals of times between each recorded event should be. This function can take into account the background radiation activity and other non-fission radiation activities from the source. From this analysis, it is possible to extract 5 parameters, which are the probability to detect the prompt γ-ray cascade from a fission, the source fission rate, the mean life of a neutron in the salt-D_2O solution, the non-fission activity from the detector and the source and (the first goal of this analysis) a neutron capture detection efficiency.

In this thesis, we will first study the characteristics of the Cf source activity, such as the sequence of the events using the neutron multiplicity of a fission. And we will also look at the interaction of the neutrons when they are scattering into the salt-D_2O solution. Based on the above information, we will build a probabilistic function $\mathcal{S}(t, t')$, which gives the probability to find a detected event spaced by a time interval greater than t compared to the previous detected event and a time interval greater than t' with respect to the next detected event.

In Chapter 3, we will learn how the data from the Cf source calibration is converted in a distribution of the time intervals between the events. The distribution array can then be compared with the function $\mathcal{S}(t, t')$. We will see how a fit is performed between the theoretical function $\mathcal{S}(t, t')$ and the experimental time interval distribution. The

results of the fits with the 5 free parameters given above, and the results of the fits by fixing the source fission rate and allowing the 4 other parameters to be free will be presented. These results are only for data recorded when the source is at the centre, because at this stage of the analysis development, we do not want neutrons going out of the acrylic vessel, where the neutron mean life is different outside the salt-D_2O medium.

Following the main results of the analysis, in Chapter 4, we will summarise the other developments in attempt to improve the method. Since the Time Series analysis is very dependent on the neutron multiplicity of the fissions, we have used other neutron multiplicities from other references to determine how significant are the changes in the results due to multiplicity distributions. In addition, we have also applied the Time Series analysis to AmBe calibration source data to extract the neutron mean life under a different chronology of the events. Also, we tried to compare the energy spectrum of the first fission event with subsequent events in attempt to find the prompt γ-ray cascade fraction over all first detected events. In the fourth section, we fitted the data with the source at some off-centre positions where we believe that the neutron diffusion volume is still contained inside the acrylic vessel.

Finally, we will summarise some of the work using the Multiplicity Method on the Salt Phase data and try to explain the limitation of this kind of analysis when applied to this experimental phase of SNO.

Chapter 2

The Theory Leading to the Californium Time Series Model

The Time Series model is essentially based on our knowledge about the californium fission characteristics and the neutron diffusion. This information leads us to a mathematical model of the event detection sequence that depends on source strength, background and detection efficiencies.

2.1 The Californium Source and the SNO Detector

To build our model, we need to understand carefully the physical situation during a calibration period of data at SNO. The scenario that we analyse in this work is the case where a Cf source is placed inside the acrylic vessel (AV) of the SNO detector. Thus, the PMTs record the activity from the source, an activity which is essentially coming from the neutrons emitted by the source.

2.1.1 The Activity from the Californium Source

The source used for the neutron calibration contains californium; the activity comes essentially from the ^{250}Cf and ^{252}Cf. These radioactive isotopes are encapsulated into a small acrylic cylinder [8]. The main characteristic of the ^{252}Cf is that it is a intense source of neutrons.

From table (2.1), we see that the main decay mode is the α decay by far. But the alpha particles emitted from Cf are rapidly stopped inside the source material, such that the detector does not see this decay. On the other hand, in the case of a fission, two daughter isotopes are produced, with a few high energetic neutrons and usually with a prompt γ-ray cascade. As for the α particles, the daughter products from the fissions are also contained inside the source and are not detected. But γ-rays and neutrons easily escape the source and are detected in the salt heavy water. Also, the daughter isotopes from the fission can also be radioactive, such that delayed radiations can be emitted, such as β-rays, γ-rays and neutrons. The only information about the activity rate of the different isotopes was done on January 15, 1998, when the source was made. It shows that the ^{250}Cf and the ^{252}Cf decay rate are at least ten times higher than the other Cf isotopes. Because the fission branch percentages of the ^{248}Cf, ^{249}Cf and ^{251}Cf are also extremely small or null, it is clear that the ^{250}Cf and the ^{252}Cf are the two dominant source of neutrons.

Since the α particles are stopped inside the source, only Cf fission products (prompt and delayed) are detected, even if the α decay is the main branch. But the Time Series model that we built is directly dependent on neutron multiplicity of each kind of fission. For this reason, it is important to check if some products from the α decays can become a significant source of neutrons. The α decays of Cf give curium (Cm). Table (2.2) shows the characteristics of Cm resulting from the 5

Isotope	Half-life (years)	α decay branch	Spontaneous fission branch	Average neutron multiplicity per fission
^{248}Cf	0.913	99.9971%	0.0029%	N/A
^{249}Cf	351	100%	4.4×10^{-7}%	N/A
^{250}Cf	13.08	99.923%	0.077%	3.511±0.037
^{251}Cf	898	100%	null	N/A
^{252}Cf	2.645	96.908%	3.092%	3.7676±0.0047

Table 2.1: Some decay characteristics of the 5 most stable Cf isotopes [9]. The average neutron multiplicity refers only to the fission branch. No other Cf isotopes can be present in significant amount in the source because of their very short half-lives.

Isotope	Half-life (years)	α decay branch	Spontaneous fission branch
^{244}Cm	18.10	100%	1.371×10^{-4}%
^{245}Cm	8500	100%	6.1×10^{-7}%
^{246}Cm	4730	99.974%	0.0263%
^{247}Cm	15,600,000	100%	null
^{248}Cm	340,000	91.74%	8.39%

Table 2.2: Decay characteristics of the 5 Cm isotopes resulting from the α decay from the Cf isotopes of the previous table [9].

isotopes shown in table (2.1). Because the half-lives of Cm isotopes are very large for most of them, the Cm fission and the production of plutonium by α decay are neglectable. For the ^{244}Cm, which has a shorter half-life, the fission branch is very small and the result of an α decay gives a ^{240}Pu with a long half-life of 6563 years [9]. Thus, no products from the α decay can be a significant neutron emitter, and we do not have to focus our attention on the α decays anymore. And only the fission process needs to be studied in detail.

The daughter products, in this case, are not as simple as the α decay products. Figure (2.1) shows that a large number of different isotopes are made by ^{252}Cf fissions. The pattern is similar for any other heavy isotopes. Obviously, some of the products

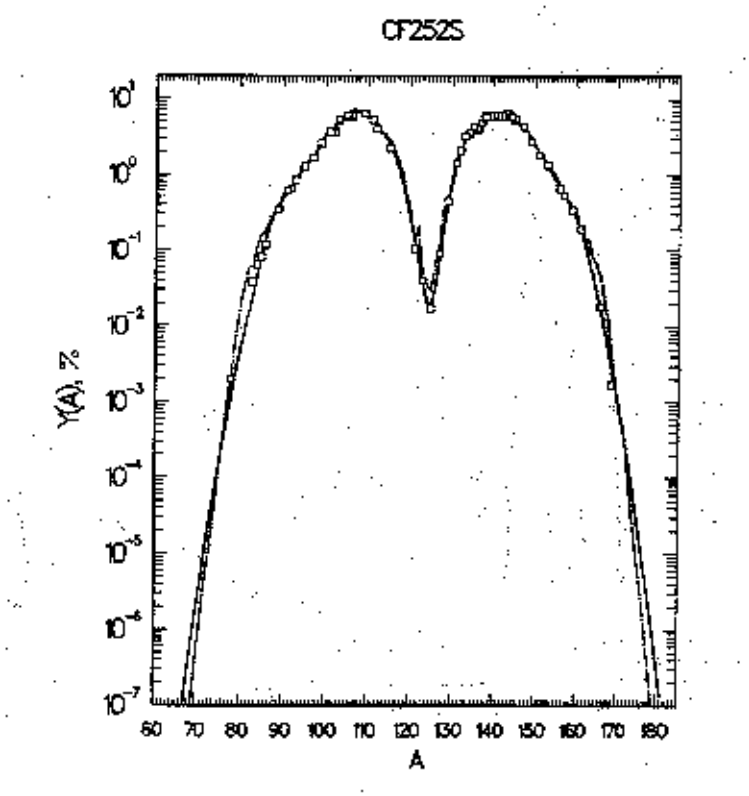

Figure 2.1: The graph from [10] shows mass number yields, Y(A), versus the mass number, A, for the fission product of ^{252}Cf. It can be seen that the fission produce a large variety of isotopes, some stable and others not.

can be unstable and then become a new source of radiation. As explained before, any α decay will not be detected, but β, γ and neutron radiations can be. To get a correct neutron detection efficiency, the model need to count properly the delayed neutrons from the daughter isotopes, but it must also exclude the β-ray and γ-ray source activity. The β-rays are rapidly absorbed in the acrylic, but they produce Čerenkov light which can be detected. In the case of γ-rays, they easily escape into the salt heavy water where they Compton scatter, and are the main source of noise.

The Shielded Source

In August 2001, the Cf source was canned in a stainless steel shield of a few millimeter thickness to reduce the emission of Čerenkov light from the β-rays, which are undesired in a neutron detection calibration. Thus, all calibration runs recorded before August 2001 are supposed to show a higher rate of non-neutron events than the runs recorded after. But the neutrons should not be absorbed by the shield such that they can cross easily outside the shield to scatter in the heavy water. The neutron activity of the source is then not affected.

2.1.2 The Diffusion in the Salt Heavy Water

In addition to the source characteristics, it is also important to study the medium where the neutrons are detected. In the Salt-D_2O experiment phase, the medium is a reservoir of heavy water where some NaCl is dissolved. Table (2.3) shows the abundance of the main isotopes present, and their thermal neutron capture cross section. The salt was added in a concentration of about 0.196g/100g of solution. It is to increase the neutron absorption inside the AV with the high cross section of ^{35}Cl. The neutron detection efficiency is then better than the pure D_2O experiment phase. The energy emitted by ^{36}Cl after a neutron is absorbed by ^{35}Cl is about 8.58 MeV, a high energy signal easy to detect. The absorption on ^{2}H, the second most probable capture, can also be detected with 6.26 MeV, but not in the case of an absorption on ^{1}H, where a signal of 2.22 MeV is lost within the low energy radiation background.

From the fissions, the source expels high energetic neutrons. These neutrons are rapidly thermalised in the water by scattering. When thermalised, neutrons diffuse randomly in the salt heavy water until they are captured, generally by a ^{35}Cl. The time interval between the fission and the capture is called the neutron lifetime. The

Isotope	N/N_{water}	σ_a (mb)	σ_a/N_{water} (mb)
^{1}H	18.32×10^{-4}	332.6	0.6093
^{2}H	1.9982	0.519	1.0371
^{14}N	3.687×10^{-5}	1905	0.0702
^{16}O	0.9963	0.190	0.1893
^{17}O	4.85×10^{-4}	235.5	0.1142
^{18}O	3.20×10^{-3}	0.16	0.0005
^{23}Na	6.72×10^{-4}	530	0.356
^{35}Cl	5.09×10^{-4}	44090	22.46
^{37}Cl	1.63×10^{-4}	433	0.0705
Total			**24.9**

Table 2.3: Abundance and neutron absorption cross section of the isotopes present in the salt heavy water tank. The numbers of Na and Cl per water molecule correspond to a concentration of 0.196 g of NaCl/100g of solution. [6, 11, 12]

time length distribution of neutron lifetimes follows an exponential, a curve similar to radioactive decay. Using the total cross section per water molecule σ_a/N_{water} in table (2.3), the density of molecules ρ_{water} and the standard thermal neutron velocity v (=2200m/s), we can estimate with equation (2.1) and (2.2) the mean life τ for the neutrons:

$$\begin{aligned} \Sigma_a &= \frac{N_A\ \rho_{water}}{M_{water}} \frac{\sigma_a}{N_{water}}, \qquad (2.1) \\ &= \frac{N_A \times 1.10 g/cm^3 \times 24.9 \times 10^{-27} cm^2}{20.0 g/mol} = 8.25 \times 10^{-4} cm^{-1}, \\ \tau &= \frac{1}{\Sigma_a v} = 5.5 ms. \qquad (2.2) \end{aligned}$$

With the theory about the diffusion of thermal neutrons [13] applied to the steady state point source, it is also possible to estimate the diffusion length L by using the neutron scattering mean free path λ in the salt heavy water (=2.4 cm for pure D_2O). Let $n(\mathbf{r})$ be the density of thermal neutrons as function of position. With the spherical symmetry of the detector, we have for the steady state point source at the origin (see

Segrè [13], eqn 12-7.2)

$$D\frac{1}{r}\frac{\partial^2}{\partial r^2}rn(\mathbf{r}) - \frac{n(\mathbf{r})}{\tau} = 0, \tag{2.3}$$

where D is the diffusion coefficient, which is

$$D = \lambda v/3. \tag{2.4}$$

With the solution for the neutron density in (2.3)

$$n(\mathbf{r}) = \frac{e^{-r/\sqrt{D\tau}}}{4\pi D\tau r}, \tag{2.5}$$

we can integrate it from the origin to a radius R. Then, we get

$$N(R) = 4\pi \int_0^R n(r)r^2 dr = 1 - (1 + \frac{R}{L})e^{-\frac{R}{L}}, \tag{2.6}$$

with

$$L = \sqrt{D\tau} = \sqrt{\frac{\lambda\, v\, \tau}{3}} \approx 31cm. \tag{2.7}$$

The interest of (2.6) is that we can know the fraction of neutron contained in a radius R. Thus, 99.0% of the neutron are absorbed inside a radius of about 206 cm, and 99.9% inside approximately 286 cm. Other documents in SNO use $L = 34$ cm, probably by taking into account each isotope scattering cross section instead of only the pure D_2O in our estimate. However, the last calculations show us that the neutrons diffuse in a smaller volume than the AV's volume. On figure (2.2), we plot the event distribution as a function of the radius from a typical calibration run with the source at centre. It can be seen that the events from the source are mostly absorbed before 400 cm. From 400 cm to 600 cm, the region is dominated by background coming from the light water, outside of the AV.

Thus, we can expect that all the neutrons are absorbed in the salt heavy water if the source is anywhere less than 350 cm from the centre of the AV. This will simplify

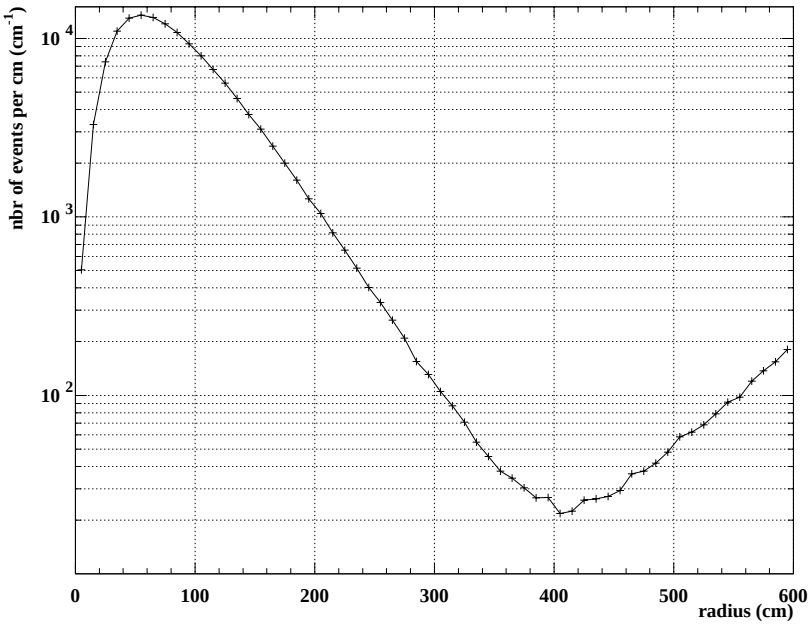

Figure 2.2: Radial distribution of events during the calibration run 21023. The source was placed at the centre during 24 hrs. We can see that the events from the source are absorbed within less than 400 cm. Beyond 400 cm, the curve shows that the events recorded come from the background activity outside of the AV.

our calculations to build the Time Series model. In the pure D_2O phase, it was not possible that all neutrons would be contained inside the AV, wherever the source position is.

2.1.3 A Typical Event Chronology

Finally, to properly use all of the information above, we can summarise it as follows: consider a typical Cf fission emitting a prompt γ-ray and 4 neutrons. First, the γ-ray will exit out of the source at the speed of light and Compton scatter with the matter by electromagnetic interaction, producing a cascade of other γ-rays and high energy electrons. The high energy electrons produce Čerenkov light that is picked up by the

PMTs in a time such that the prompt γ-cascade detection coincides with the time of the fission.

Following the γ-rays, the 4 high energetic neutrons scatter out of the source, rapidly losing their energies and start a thermal diffusion into the salt-D_2O solution. With a mean life of about 5.5 ms and a diffusion length of about 31 cm, the 4 neutrons are captured one after the other by the ^{35}Cl within probably 10ms and inside a radius of 150 cm around the source. The absorption emits one or more γ-rays, by de-excitation of the ^{36}Cl. These new γ-rays, in their turn, produce Čerenkov light to be detected by the PMTs, depending on the efficiency of the detector.

After this series of events related to one fission, the detector waits a few tenths of a second on average before the next event. This next event might be another fission, a background event or an event related to a fission daughter product. In the two last cases, the event will probably be isolated by a time gap of tenths of a second. And after, when the next fission happens, the detector should record again a few events in few milliseconds. The fact that several events in a short period are detected when a fission occurs makes the distinction between background and fission events easy.

The consequence of this chronology is that a calibration run using the Cf should show two typical interval of times: (a) some successive short intervals of a few milliseconds, related to a single Cf fission, and (b) some long intervals of a few tenths of a second, related to pairs of fissions, independent background events or some non-fission decays from the source. This is the main assumption leading to the Time Series analysis.

2.2 The Survival Function

The waiting time probabilities between each event is represented in our model by the "survival equation". This equation, $\mathcal{S}(t)$, is defined as the average count rate of time intervals greater than t. The survival equation can be considered as the heart of the Time Series model. Because of its importance, we show on the next pages the steps leading to the equation. The following summarises the demonstration of the survival equation in [14].

2.2.1 The Survival Function for a Single Fission

Let us begin with the simple case: a single fission with n neutrons emitted and preceded by a prompt γ-ray cascade. The γ-ray cascade, if detected, is then seen at the same time as the fission occurs. Let γ be the probability to detect a prompt γ-ray cascade (be careful with the notation: "γ" is a probability, not a "γ-ray"). Suppose that the γ-ray cascade is detected, then the interval of time after terminates with the detection of one of the n neutrons.

The probability for a neutron to be captured after a time t after fission follows an exponential function: $e^{-t/\tau}$, where τ is the neutron mean lifetime when diffusing into the salt-D_2O solution. The probability that a neutron is captured within the same time t is $1 - e^{-t/\tau}$. Let ϵ be the neutron capture detection efficiency of the detector, the probability that the neutron is captured and detected is $\epsilon(1-e^{-t/\tau})$. The difference from unity, i.e. $1-\epsilon+\epsilon e^{-t/\tau}$, is the survival equation: the probability that a waiting time interval starting with prompt γ-ray detection will not be terminated within a time t. This probability is for one neutron. In the case of n neutrons, each neutron has an independent history such that the survival probability can be

written as $(1-\epsilon+\epsilon e^{-t/\tau})^n$. Now, if we consider that the γ-cascade is detected with a probability γ, the probability to have waiting times of magnitude greater than t becomes

$$S^{(1)}_{\gamma ray}(t) = \gamma\,(1-\epsilon+\epsilon\,e^{-t/\tau})^n. \tag{2.8}$$

The superscript (1) on S means that the equation is for 1 fission.

Now, a similar demonstration can be done for the subsequent time intervals between the n neutrons of the single fission. Here, all intervals begin and end with a neutron detection. Suppose the first neutron capture is detected, the following interval will be similar to equation (2.8), with the substitutions $\gamma \rightarrow n\epsilon$, because the detection efficiency is now that for a neutron and the first capture could be any of the n neutrons, and $n \rightarrow n-1$, because we have one less possible neutron following the first neutron capture. Then we get $n\epsilon(1-\epsilon+\epsilon e^{-t/\tau})^{n-1}$.

We must also take into account that all neutrons must have survived at the time of first neutron capture since the fission time. Let s be the time between the fission and the first neutron capture, the time distribution for the probability of no capture for the n neutrons is $e^{-ns/\tau}ds/\tau$. Since the first neutron capture can occur at any time after the fission, we must integrate the probability distribution from $s=0$ to $s=\infty$. The survival equation for the time interval between the first and next neutron capture becomes

$$\begin{aligned} S^{(1)}_{1^{st}\,neutron}(t) &= \int_0^\infty ds\,\frac{e^{-ns/\tau}}{\tau}\,n\,\epsilon\,(1-\epsilon+\epsilon\,e^{-t/\tau})^{n-1}, \\ &= \epsilon\,(1-\epsilon+\epsilon\,e^{-t/\tau})^{n-1}. \end{aligned} \tag{2.9}$$

For the time intervals following the subsequent neutron captures, we get logically

$$\begin{aligned} S^{(1)}_{2^{nd}\,neutron}(t) &= \epsilon\,(1-\epsilon+\epsilon\,e^{-t/\tau})^{n-2}, \\ S^{(1)}_{3^{rd}\,neutron}(t) &= \epsilon\,(1-\epsilon+\epsilon\,e^{-t/\tau})^{n-3}, \end{aligned}$$

$$\vdots$$

$$S^{(1)}_{m^{th}\ neutron}(t) \;=\; \epsilon\,(1-\epsilon+\epsilon\,e^{-t/\tau})^{n-m}.$$

As a check, the last neutron is not followed by any other event, such that if we detect the last neutron ($m = n$ and put $\epsilon = 1$ to simplify), the probability for a time interval greater than t is 1, as the interval of time is infinite. The result of all possible detection possibilities is a geometrical series and gives

$$\begin{aligned} S^{(1)}_{neutron}(t) &= \epsilon \sum_{m=1}^{n} (1-\epsilon+\epsilon\,e^{-t/\tau})^{n-m}, \\ &= \epsilon\,\frac{1-(1-\epsilon+\epsilon\,e^{-t/\tau})^{n}}{1-(1-\epsilon+\epsilon\,e^{-t/\tau})}, \\ &= \frac{1-(1-\epsilon+\epsilon\,e^{-t/\tau})^{n}}{1-e^{-t/\tau}}. \end{aligned} \tag{2.10}$$

The sum of (2.8) and (2.10) is the survival function (2.11), which is the average number of detected events, for a single fission that produces n neutrons and maybe a prompt γ-cascade, in which the time interval following detection survives to times greater than t:

$$S^{(1)}_{n}(t) = \gamma\,(1-\epsilon+\epsilon\,e^{-t/\tau})^{n} + \frac{1-(1-\epsilon+\epsilon\,e^{-t/\tau})^{n}}{1-e^{-t/\tau}}. \tag{2.11}$$

In the limit case $t \to 0$, the function counts all intervals, and the result gives the average number of detections for a fission emitting n neutrons:

$$S^{(1)}_{n}(0) = \gamma + n\epsilon. \tag{2.12}$$

2.2.2 The Survival Function for Many Fissions

The next step leading to the Time Series model is to extend the survival function to many fissions. First, the probability for a fission to produce n neutrons is given by a neutron multiplicity distribution, specific for each isotopes. For example, with a

mean multiplicity of 3.767 neutrons per fission, the ^{252}Cf has more chance to emit 3 or 4 neutrons per fission than any other numbers. Thus, the survival equation must be weighted according to the neutron multiplicity probabilities. If f_n is the probability for a multiplicity of n neutrons, we get for any fission case

$$S^{(1)}(t) = \sum_{n=0}^{\infty} f_n \, S_n^{(1)}(t). \tag{2.13}$$

If we consider now the fissions over the time line, with a finite fission rate λ, the probability that the next fission occurs in a time greater than t would be $e^{-\lambda t}$. But in our experimental conditions, the probability to record a same interval must be greater since some fissions are not detected, i.e. none of the γ-ray cascade and the neutrons from the fission are detected. We can replace t in the exponential by a function $T^{(1)}(t)$ which takes into account the detection probabilities. Details of the derivation of $T^{(1)}(t)$ can be found in the appendix in [14]. The average number of time intervals per fission of magnitude greater than t becomes

$$S(t) = S^{(1)}(t) \, e^{-\lambda T^{(1)}(t)}, \tag{2.14}$$

where

$$T^{(1)}(t) = \int_0^t dt' \, S^{(1)}(t') = \sum_{n=0}^{\infty} f_n \int_0^t dt' \, S_n^{(1)}(t'). \tag{2.15}$$

The integral in (2.15) can be done explicitly for our model, to get

$$\begin{aligned} T^{(1)}(t) \;=\; & \sum_{n=0}^{\infty} f_n \{ [1 - (1-\gamma)(1-\epsilon)^n] \; t \\ & -\tau \sum_{m=1}^{n} \left(\begin{array}{c} n \\ m \end{array} \right) \frac{\epsilon^m}{m} \left[(1-\gamma)(1-\epsilon)^{n-m}(1 - e^{-mt/\tau}) + (e^{-t/\tau} - 1)^m \right] \}. \end{aligned} \tag{2.16}$$

The next step is to take into account the background. We consider as background any other events that are not from a fission. In our model, we supposed that there is no correlation between times of background events and times of fissions, such that

the events happen following an independent average rate λ_b. We also consider no correlation between two background events. If $\lambda S(t)$ is the average count rate of intervals greater than t for fissions only, the new average count rate $\mathcal{S}(t)$ (a calligraphic S) becomes

$$\mathcal{S}(t) = [\lambda_b + \lambda S^{(1)}(t)]\, e^{-\lambda_b t - \lambda T^{(1)}(t)}. \tag{2.17}$$

It gives the average count rate of intervals with magnitude greater than t. $\mathcal{S}(t)$ has 5 unknown constants which we will be able to fit as free parameters to the data arrays. These parameters are the probability to detect a prompt γ-cascade γ, the neutron detection efficiency ϵ, the fission rate λ, the background rate λ_b and the neutron mean life τ.

The Total Number of Detected Events

The total number of detected events $\mathcal{D}$ within a time period $\mathcal{T}$ of data can be obtained from (2.17) by counting all intervals, i.e. calculating $\mathcal{S}(0)$. The detection rate is

$$\frac{\mathcal{D}}{\mathcal{T}} = \mathcal{S}(0) = \lambda_b + \lambda(\gamma + \mu\epsilon), \tag{2.18}$$

where μ is the mean neutron multiplicity ($\mu = \sum_n n f_n$). This relation is very interesting since we know exactly from a period of data, its time length and how many events are recorded, and thus the left side of (2.18). If μ is fixed by a model independently of the Time Series analysis, then (2.18) becomes a constraint on the 4 parameters λ_b, λ, γ and ϵ.

2.2.3 The Joint Survival Function

The survival function $\mathcal{S}(t)$ would not be enough to find efficiently the 5 unknown constants. For example, even if we know the rate of long time intervals, from gaps

between fissions and background, and the rate of small intervals, from waiting times between the neutrons and γ-rays of a same fission, it is not easy to separate the background rate and the fission rate. But if we consider that background events are usually isolated in time, then the event should be separated by long intervals before and after. This is not the case for typical fissions since they form groups of close events, such that for a event of the group, it cannot be separated by long intervals on both sides. For this reason, it becomes interesting to make a joint distribution of successive waiting times, before and after an event.

Consider the single fission case to get the joint survival function $S_n^{(1)}(t,t')$, where t is the time preceding, and t' the time following a detection. Suppose we have an event from this fission with time intervals before and after greater than t and t' respectively. If the event is the γ-cascade, there is no possibility for this event for a preceding detection. Thus, $S_{\gamma ray}^{(1)}(t)=1$ and $S_{\gamma ray}^{(1)}(t')$ is the same as (2.8):

$$S_{\gamma ray}^{(1)}(t,t') = \gamma\,(1-\epsilon+\epsilon\,e^{-t'/\tau})^n. \tag{2.19}$$

Now let us consider an event which is one of the n neutrons, with the fission having occurred at time s. In the case where s is within an interval (0,t) before the detected event, then no other detection are possible until a time $s+t'$ after fission. First, the probability of detection of this neutron is $n\epsilon$. Second, the γ-rays must not be detected: $(1-\gamma)$. Third, the probability for the $n-1$ remaining neutron not to be detected until t' after our detection is $(1-\epsilon+\epsilon e^{-(s+t')/\tau})^{n-1}$. Fourth, because s can take any value in the interval (0,t), we must integrate it to get a complete equation:

$$\begin{aligned} S_{neutron,1}^{(1)}(t,t') &= n\,\epsilon\,(1-\gamma)\int_0^t \frac{ds}{\tau}\,e^{-s/\tau}\,(1-\epsilon+\epsilon e^{-(s+t')/\tau})^{n-1}, \\ &= (1-\gamma)\,e^{t'/\tau}\,[(1-\epsilon+\epsilon e^{-t'/\tau})^n-(1-\epsilon+\epsilon e^{-(t+t')/\tau})^n]. \end{aligned} \tag{2.20}$$

In the last case, we have again the same detected neutron, but now the fission has

occurred outside the (0,t) interval. The detection or not of the γ-rays is now irrelevant since it must happen outside our interval. For the $n-1$ remaining neutrons, they must not be detected in the interval (s,s+t+t') after fission. The survival function becomes

$$\begin{aligned} S^{(1)}_{neutron,2}(t,t') &= n\,\epsilon \int_0^\infty \frac{ds}{\tau}\, e^{-(s+t)/\tau}\,(1-\epsilon\, e^{-s/\tau}+\epsilon e^{-(s+t+t')/\tau})^{n-1}, \\ &= e^{-t/\tau}\,\frac{1-(1-\epsilon+\epsilon e^{-(t+t')/\tau})^n}{1-e^{-(t+t')/\tau}}. \end{aligned} \tag{2.21}$$

The sum of (2.19), (2.20) and (2.21) lead to

$$\begin{aligned} S^{(1)}_n(t,t') &= \gamma\,(1-\epsilon+\epsilon\, e^{-t'/\tau})^n + \\ &\quad (1-\gamma)\, e^{t'/\tau}\,[(1-\epsilon+\epsilon e^{-t'/\tau})^n-(1-\epsilon+\epsilon e^{-(t+t')/\tau})^n] + \\ &\quad e^{-t/\tau}\,\frac{1-(1-\epsilon+\epsilon e^{-(t+t')/\tau})^n}{1-e^{-(t+t')/\tau}}, \end{aligned} \tag{2.22}$$

$$S^{(1)}(t,t') = \sum_{n=0}^{\infty} f_n\, S^{(1)}_n(t,t'), \tag{2.23}$$

and

$$S(t,t') = S^{(1)}(t,t')\, e^{-\lambda\, T^{(1)}(t+t')}. \tag{2.24}$$

The argument for the exponential factor in (2.24) is exactly the same as in (2.14), except that here the time interval in which nothing is to be detected is $t+t'$ rather than just t.

Finally, we must include the background rate into (2.24). In this more complex case, the substitutions are $\lambda\, S^{(1)}(t,t') \to \lambda_b + \lambda\, S^{(1)}(t,t')$ and $\lambda\, T^{(1)}(t+t') \to \lambda_b\,(t+t') + \lambda\, T^{(1)}(t+t')$ and we get the average count rate

$$\mathcal{S}(t,t') = [\lambda_b + \lambda S^{(1)}(t,t')]\; e^{-\lambda_b\,(t+t')-\lambda\, T^{(1)}(t+t')}. \tag{2.25}$$

Example with a Single Fission Emitting 1 γ-ray and 1 Neutron

To give us a clearer idea about the meaning of equation (2.22), let apply it with a simple case: a single fission emitting 1 γ-ray and 1 neutron. Then, $n = 1$ and $S_n^{(1)}(t, t')$ is reduced to

$$S_1^{(1)}(t, t') = \gamma + \epsilon - \gamma\epsilon(2 - e^{-t/\tau} - e^{-t'/\tau}). \tag{2.26}$$

We must remember that $S(t, t')$ is the average number of events with a time interval greater than t before the event itself and greater than t' after it. In our case, it has a possibility to detect 1 or 2 event(s), but not 0 because $S(t, t')$ is always relative to a detected event. So at least 1 event must be detected. With 1 or 2 event(s), we have a possibility of 2 or 3 time intervals related to the fission.

To interpret the physical meaning of (2.26), it is helpful to rearrange it in 2 parts:

$$S_1^{(1)}(t, t') = \gamma[1 - \epsilon(1 - e^{-t'/\tau})] + \epsilon[1 - \gamma(1 - e^{-t/\tau})]. \tag{2.27}$$

The first part represents the case when the event we are looking at is the γ-ray: the probability to detect it is γ; if the neutron is not detected, than the probability for time intervals greater than t before and t' after is 1; and we subtract the probability to detect a neutron within t', i.e. $\epsilon(1 - e^{-t'/\tau})$. The second part is the same idea, but in the neutron event case and looking backward for any γ-ray closer than t.

Chapter 3

The Data Analysis using the Time Series Model

Having set up the Time Series model for neutrons coming from the californium source, we are ready to analyse the experimental data from SNO's data bank. The analysis presented in this chapter will show what the neutron detection efficiency is for SNO's Salt-D_2O phase using our Time Series analysis. Also, the source fission rate, the source strength, the neutron mean life, the prompt γ-ray detection probability and the background activity will be extracted in the analysis.

3.1 The Data Handling

The process to find the neutron detection efficiency is divided into two main parts:(a) the data in the ROOT files are read to make Time Series distribution arrays and (b) these arrays are fitted by the theoretical equation of the Time Series model.

3.1.1 The SNO Data Selection

The data from the SNO calibration runs are divided in many periods. One run cover a period of time where the detector is under the same experimental conditions. The runs are available under two data formats: the "zdab" and the "ROOT" files. The zdab are the raw data recorded directly from the detector. But for our analysis, we need more information than the zdab files provide, such as the position and the total energy of each event. The ROOT files are extracted from the zdab files and provide more information. In the "rootification", the ROOT files production, some primary analysis are done from the zdab data. From the information recorded from each PMTs in the zdab files, the rootification makes some fit which can provide the event positions and their total energy. These values are then available for each event in the ROOT files. We have used the ROOT data files for our analysis. More information about the ROOT format can be found in [15].

For each neutron calibration run, the Cf source has a fixed position inside the AV (acrylic vessel). At this stage, the Time Series model is limited to the runs where the source is near the centre of the AV. Also, for significant statistics, we keep in our data selection only runs of more than 1 hour in duration. After investigation through all californium shift reports, we found 8 ROOT files satisfying our conditions and also without problems. Table 3.1 shows our data selection.

We can see from the table that the source is generally not exactly at the centre. The main importance about the radial position is that the neutron must not go through the AV. In the salt-D_2O medium, the neutron does not diffuse significantly beyond 300 cm, as shown in figure (2.2). So an off-centre source by a few centimeters (like 22cm in our case) will not change the result as long as the neutrons are kept inside the AV.

ROOT files	Date (dd/mm/yy)	nbr of days since June 12, 2001	radial position (cm)	time length (sec)
SNO_020731_p1.root	30/07/01	48	0	27950
SNO_021023_p1.root	09/09/01	89	22	86402
SNO_022348_p1.root	17/11/01	158	22	46825
SNO_022349_p1.root	18/11/01	159	22	38762
SNO_022669_p1.root	19/12/01	190	22	3643
SNO_022942_p1.root	15/01/02	217	22	3626
SNO_025707_p1.root	20/06/02	373	1	7204
SNO_028535_p1.root	14/01/03	581	2	28820

Table 3.1: 8 runs show the Cf source at centre for more than 1 hour. Version "p1" (in the ROOT file name) is a rootification update done in April 2003 following the last available information about the detector electronics.

Since the source strength has been measured independently in Los Alamos National Laboratory on June 12, 2001 [16] , we show in the table the number of days passed since that day for each run to compare later between ours and LANL's source strength.

3.1.2 The Calculation to Make Arrays

The next step of the work was to make a Time Series array which can show the distribution of the time intervals between the events. The obtained matrix will contain all the information from the run events that is needed to extract all our unknown parameters from the Time Series theory.

To make the arrays, we had to extract from the ROOT files all events recorded and check their position, their energy and their time. To be captured as a count event, each event had to be inside the acrylic vessel ($<$ 600 cm from centre) and above a predetermined energy threshold. It means that only the events above the energy threshold and inside the 600 cm radius have been used to fill the matrix.

For each run, the analysis has been done with 10 different energy threshold cuts:

from 2.5 MeV to 7.0 MeV by steps of 0.5 MeV (in total energy of the events). The energy value that we use throughout this work is the total energy response of the detector when electrons make Čerenkov light. The energy response E_{RSP} is related to the electron kinetic energy E_{KE} by this relation:

$$E_{RSP} = E_{KE} + 0.511\, MeV. \tag{3.1}$$

At low energy thresholds, we can capture most events from the Cf source, but the background contamination is expected to be high. At higher energy thresholds, the background activity should decrease and eventually vanish but a lot of events from the source will also be missed. By covering different energy thresholds, we can then see how disturbing the varying presence or the absence of events such as the background, the prompt gamma rays from the source, or a low neutron detection efficiency can affect the quality of our results. SNO is particularly interested in energy thresholds around 5.5 MeV, which is the energy region they expect to use as neutrino energy threshold for the neutrino analysis.

To read the time, we have tried to be very careful to not lose any precision during the array calculations. In the ROOT files, the time is divided into three segments: the Julian date, the time within the day shown in seconds (technically called UT1 here, for Universal Time, part 1) and the fraction of time within this second, accurate to 100 nsec (called UT2). The time of each selected event had to be compared with the previous event without losing this 100 nanoseconds accuracy. To do that, each time segment of a selected event has been subtracted by the corresponding time segment from the previous event such that the numbers compared were not too big for a "double variable" (Float 8 bytes). Then, it is only the calculated difference between each segment which are summed together (after conversion in μsec) to get a interval of time, Δt, for the array.

At each captured event, we checked the interval of time which separates the event from the previous captured event and the next captured event. The time separation before and after a specific event was used to choose the position on a two-dimensional square matrix: the horizontal axis representing the time interval before the event and the vertical axis for the time separation with the next event.

The size of the array is $26X26$. To fill an array we used an equation following this logic:

$$column\ \# = 5log_{10}(\Delta t_{before}) - 6, \tag{3.2}$$

$$row\ \# = 5log_{10}(\Delta t_{after}) - 6, \tag{3.3}$$

where the intervals Δt are given in μsec. From these equations, we take the integer parts of the answer as the column or row number, the first column or row being #0. The first and last columns and rows are special bins such that the first bin (0,0) includes all events having a time separation less than 25.12 μsec before and after, and the last bin (25,25) shows how many events have a time interval bigger than 1.58 sec with the previous and next captured events.

Beside the time intervals, a second piece of information is needed to complete our Time Series analysis: the run time length. To do this, the two first time segments, the Julian Date and UT1, from the very first event are kept in memory and are compared at the end with the Julian Date and UT1 from the very last event read by the programme. UT2 is a negligible time scale compared to runs of more than an hour, so it was not used for the run time length.

After having sorted all time intervals of captured events and found the run time length, this information is saved in a text file: the run time length on the first line, the matrix on the 26 next lines. Then, the files are ready to be fitted. Appendix A

shows the C++ programme code used and a sample of Time Series file.

The Clearance of Some Suspect Intervals of Time

We have seen on some ROOT files some anomalies in the chronology. First, it happens in rare cases that an event has an earlier time compared to the previous event, such that our calculated interval of time will be negative! We do not have an explanation for this kind of error. Anyway, we have added in the programme a command excluding any negative intervals. These negative intervals are of the order of 1 sec, and in our analysed files, they appeared only 3 times in run period file # 22348 (let calls these "period files" "runs").

Secondly, we have also found in some rare cases very long time intervals, of the order of 100 secs. We obviously consider them as unphysical intervals. Using the Cf source fission rate, we have estimated that the probability of any time intervals above 10 secs inside 24 hours are improbable and then unphysical, and thus must be excluded in the array count. Because an exclusion of this order of time might become important compared to the run time length, the excluded large time interval is also subtracted in our measurement of the run time length. Again, this situation happened only in run 22348 in our run selection. We will come back to the run 22348 case in more detail, later.

Each Time Series file keeps a log at the end of all negative and large Δt values, in the case we need to investigate the data quality.

3.1.3 The Fitting Procedure

After having a Time Series matrix for each available run at the centre and for different energy thresholds, the next work was to perform a fit with the Time Series model

explained in the previous chapter. The calculation needed here was a longer and more complex routine than the array making routine done previously. The fit was done by a Fortran programme which directly reads the array and outputs the best parameter values found.

5 parameters can be free during the fit: the probability to detect a γ-ray as first detected fission event, the efficiency of neutron detection, the fission rate of the source, the mean life of a neutron in the D_2O, and the excess background strength.

The γ-ray probability is added in the programme because we have no idea if the first detected event from a Cf decay is a neutron or a prompt γ-ray. It is believed that in this analysis, the typical time interval between a prompt γ-ray and the first detected neutron would be slightly different compared with the two first neutrons, and that it would be possible to distinguish it. In practice, we know that it was the hardest parameter to fit. The efficiency of neutron detection is the ultimate goal of this work.

We can easily understand that this parameter is highly correlated with the prompt γ-ray probability: is the first event counted as a γ-ray or a neutron? The fission rate and the mean neutron life are less correlated and will give to us a excellent check for the consistency of the result. Finally, the excess background will show how many events are other than Cf neutrons. The excess background excludes the delayed neutrons from the radioactive products of Cf fissions.

The Fission Models

The accuracy of the Time Series model is very dependent on our multiplicity knowledge from the fissions occurring in the source. For the ^{252}Cf, we have used two different references. The first is a simple Gaussian distribution used by Dragowsky [16] for

Isotope	Half-life (years)	fission ratio on June 12, 2001	Model	Probability for n neutrons per fission
^{252}Cf	2.645	97.6%	Gaussian	$P(n) = 0.3184 gaussian(\mu = 3.767, \sigma^2 = 1.57)$
			hot fission	$P(n) = 0.3176 gaussian(\mu = 3.767, \sigma^2 = 1.57)$ $+0.0012 gaussian(\mu = 7.6, \sigma^2 = 0.8)$
^{250}Cf	13.08	2.4%	Gaussian	$P(n) = 0.3184 gaussian(\mu = 3.511, \sigma^2 = 1.57)$

Table 3.2: We try two models for ^{252}Cf whereas ^{250}Cf stays the same model everywhere in this analysis. Without references for the ^{250}Cf standard deviation, we estimate it to be the same as the ^{252}Cf one.

SNO, called the Gaussian model. The second distribution is from Ter-Akopian [17] and Wu [18], who show the presence of a hot fission mode from more recent measurements on the ^{252}Cf. We call this last the hot fission model, including a normal and a hot fission mode. For the analysis, we alternated both models, expecting that it will be possible at the end to discriminate one of them by comparing the fit quality of each.

We did not find specific references about the ^{250}Cf multiplicity as well as the ^{252}Cf. Referring to Dragowsky [16], an average neutron multiplicity is given, but not the standard deviation. After a discussion with him, the standard deviation is expected to be very close to the one from ^{252}Cf (from the the Gaussian model). Then we used the same standard deviation for both isotopes. From the same reference [16], a spontaneous fission ratio has been measured between the ^{252}Cf and the ^{250}Cf on June 12, 2001. Because the two isotopes have two different half-lives, their relative fission rates were calculated as a function of time from this date. To make a more accurate model about the ^{250}Cf, like finding the real standard deviation or search for some empirical models, was not essential as ^{250}Cf represents less than 3% of the total source neutron activity. Table 3.2 summarises our source model.

After a fission, we cannot expect at all time, the simple scenario where we detect

only the neutron emitted by the fission itself. The fission can introduce indirectly other neutrons. During the burst, we have considered two reactions with the D_2O which can be sources of extra neutrons:

$$d + n \longrightarrow p + n + n \tag{3.4}$$

$$d + \gamma \longrightarrow p + n \tag{3.5}$$

These reactions can occur from the γ-rays and the energetic neutrons emitted by the Cf source. We have estimated 0.84% of the neutrons emitted by the Cf will cause the first reaction and 0.16% of the γ-rays emitted will cause the second one [11]. Because they will occur in the neutron burst event period, those probabilities were input in the multiplicity factors. Also, the daughter products from the Cf fissions can also be sources of neutron radiation. The multiplicity factor for these delayed neutrons is 0.78% [16]. In our model, the delayed neutrons are considered to be emitted uniformly and are considered as part of the background.

The Comparison and Fitting Techniques

The fit programme works by minimising the χ^2 with the parameters that we let vary. The method used is a Newton-Raphson technique applied on the 5 free parameters. It is at this time that we use the survival equation described in the previous chapter.

First the data array is normalised to 1 hour using the run time length available in the first line of the array file. The computer then generates a model array using our input values as guesses for the 5 parameters. The model array is built by the joint survival function written in (2.25):

$$f_{kl} = counts = 3600[S(t_k, t_l) - S(t_{k+1}, t_l) - S(t_k, t_{l+1}) + S(t_{k+1}, t_{l+1})], \tag{3.6}$$

where l and k represent the lines and columns of the array. Then, a likelihood χ^2 for Poisson statistics is calculated between the model generated by our guess values and the real data as follows [19]:

$$\chi^2 = -2\sum_{k,l}[x_{kl} - f_{kl} + x_{kl}\ln(f_{kl}/x_{kl})], \tag{3.7}$$

with f as the model and x as the data. The χ^2 is calculated on empty bins, where it is $2f_{kl}$ since both x_{kl} and $x_{kl}\ln(x_{kl})$ are understood to be 0.

The best fit is defined as the fit that minimises the χ^2. To minimise, we used an approximate Newton-Raphson method. In this method, the χ^2 is expanded by a Taylor series to the second order for our 5 free parameters λ_i. The result gives this formula:

$$\chi^2 \approx \chi_0^2 + \sum_i L_i\ \delta\lambda_i + \sum_i\sum_j M_{ij}\ \delta\lambda_i\ \delta\lambda_j, \tag{3.8}$$

where χ_0^2 is the one from the previous guess, and

$$\begin{aligned}
L_i &= 2\sum_{k,l}(1 - \frac{x_{kl}}{f_{kl}})\frac{\partial f_{kl}}{\partial\lambda_i}, && (3.9)\\
M_{ij} &= \sum_{k,l}[\frac{x_{kl}}{f_{kl}^2}\frac{\partial f_{kl}}{\partial\lambda_i}\frac{\partial f_{kl}}{\partial\lambda_j} + (1 - \frac{x_{kl}}{f_{kl}})\frac{\partial^2 f_{kl}}{\partial\lambda_i\partial\lambda_j}], && (3.10)\\
&\approx \sum_{k,l}\frac{x_{kl}}{f_{kl}^2}\frac{\partial f_{kl}}{\partial\lambda_i}\frac{\partial f_{kl}}{\partial\lambda_j}, && (3.11)\\
\delta\lambda_i &= \lambda_i - \lambda_{i0}. && (3.12)
\end{aligned}$$

To simplify the calculation of M_{ij}, we kept only the part shown in (3.11). The L_i can be understood as the 5 slopes of χ^2 relative to the 5 free parameters. Then, a minimum is reached when all L_i vanish. Giving an approximate values for each $\boldsymbol{\lambda}$ (in vectorial notation), the Newton-Raphson improvement is the replacement of each $\boldsymbol{\lambda}$ by $\boldsymbol{\lambda - M^{-1}L}$. And after, it has to recalculate the χ^2 and redo the Newton-Raphson estimate until the minimum is reached (i.e. $\boldsymbol{L}$ vanishes).

The approximation of $\boldsymbol{M}$ can make the convergence harder in some cases. In the case where the convergence does not occur, we used "Minuit"(another fitting programme) as an alternative. "Minuit" is a programme within the CERN computer library package [20]. Minuit is used to minimise the χ^2 given in equation (3.7). This independent check did not show any differences to the Newton-Raphson method.

The statistical uncertainty of our result are defined as the variation which increases the χ^2 by unity. As for the degree of freedoms, it is defined in our case as the expected χ^2 minus the number of free parameters.

3.2 Presentation and Discussion on the Results

Now that we have explained the methodology of the Time Series analysis, we are ready to show the results. This section shows our main results which are the 5 free parameter fits and the 4 free parameter fits where the fission rate was fixed. But first, let us take a look at the data arrays.

3.2.1 An Interpretation of the Arrays

Making a 3D graph in figure (3.1) from an array at 2.5 MeV energy threshold cut, we can see 4 peaks of different heights making a square. Those peaks shows that each event is distributed in time, following a very clear pattern: most events are separated by two typical intervals of time before and, obviously, two typical intervals of time after. So depending if an event is separated by a long time interval before and a long time interval after (called long-long), a short-long, a long-short or a short-short interval, the events are concentrated in the corresponding peak.

Each peak gives some information about the neutron source activity. First, the

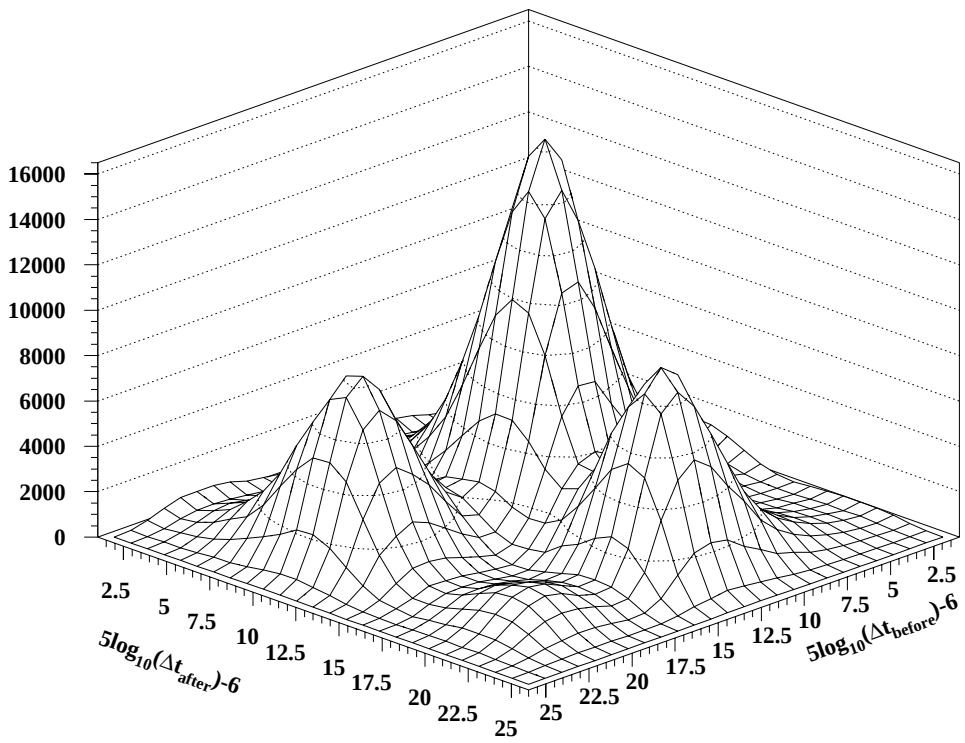

Figure 3.1: Plot of a Time Series array at 2.5 MeV energy cut from run 21023. We can see four distinctive peaks. The horizontal axis are the rows and columns calculated from equations (3.2) and (3.3), representing the time intervals before and after each event. The vertical axis is the number of events per bin.

long-short peak (the left one on the graph) includes most of the first events from a Cf fission: after an arbitrarily long period of time (order of 0.25 sec), a fission happens and the first event from the fission is detected, following immediately after (order of a few msec) by a second detected event. In opposition, the short-long peak (on right) is essentially the sum of the last detected events from a fission: just after a second last event (short time before), the last neutron is followed by a typical long interval of time until the next fission. Because we have one first event and one last event per fission (obviously!), then the short-long and long-short peaks give an idea of how

many fissions happen during the run: the integral of each two peaks should be close together and roughly equal to the number of fissions in the run.

As for the short-short peak (the high peak in the back), it should include all events happening between the first and last event from a fission. Knowing the average multiplicity of the ^{252}Cf (μ=3.767n/fission), the relative height of the short-short peak gives an idea of the efficiency of the detector. For example, in a 100% efficiency detector without prompt γ-ray detection, the short-short peak would be about 1.767 higher than the short-long and long-short peaks (1 first neutron + 1.767 intermediate neutron + 1 last neutron = 3.767 neutrons/fission). The effect of detecting sometimes prompt γ-cascades push the first detected neutron from the long-short to the short-short peak, making the short-short peak bigger. Thus, we can already see the high correlation induced between the prompt γ-rays detection and the neutron detection efficiency: they both affect the the relative size of the short-short peak, making it hard to distinguish if a change in its size comes from the prompt γ-ray detection or the neutron detection efficiency.

Finally, the long-long peak (the small one on the front) would be the sum of all independent events, distributed randomly in time. Some of those events can be a fission with only one neutron detected, but long-long peak gives especially information about the background existing during the run. This background must be the dominant kind of events in this peak, and then, we see clearly that the Time Series analysis gives an opportunity to differentiate the background from the Cf fission events.

Figure (3.2) shows how the distribution looks if the energy threshold cut jumps to 7.0 MeV. We can see that the short-short peak is very small and the long-long one becomes important. At this threshold, the background disappeared, such that the long-long peak contains essentially neutrons. Because the threshold is high, most of

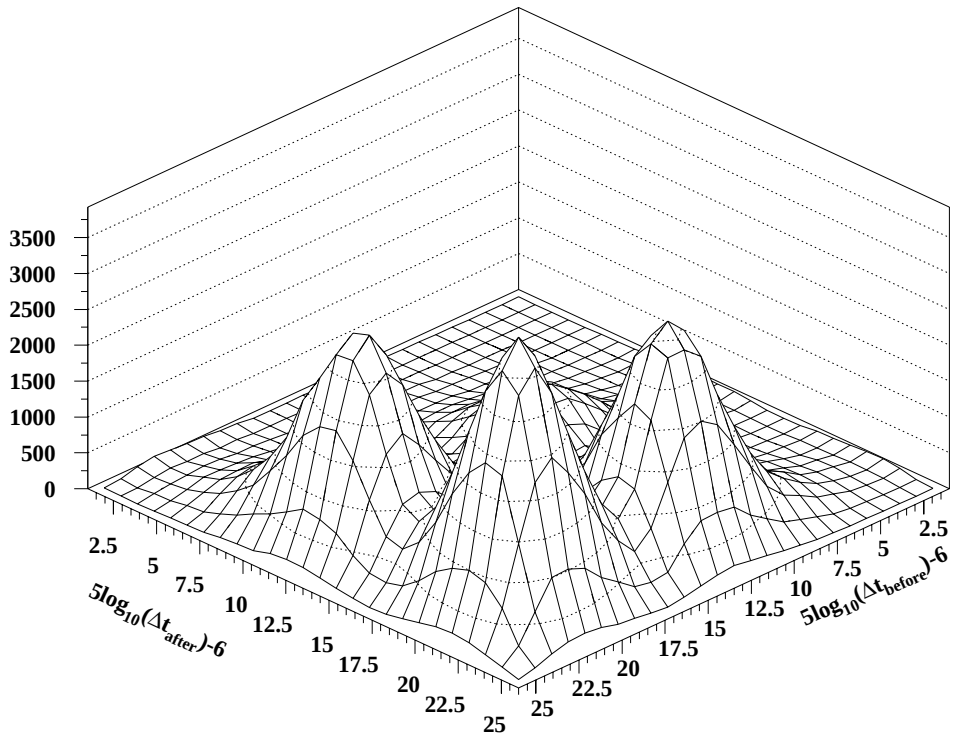

Figure 3.2: Similar plot as the previous, but at a 7.0 MeV energy cut. The long-long peak is filled even if no significant background is counted because we are more likely to count only 1 event per fission.

the events are cut out in the count, and then we are more likely to see 1 or 2 events per fissions. Thus, with 1 counted event per fission, the long-long peak is filled as if it was the isolated background events. In this case, the neutron detection efficiency is very low and the total count of events is a lot less than at 2.5 MeV.

3.2.2 The Fit Results with 5 Free Parameters

In the appendix B, you can see tables showing all the results for fits of our 8 centre runs with the 5 parameters free, from a energy threshold cut of 2.5 Mev to 7.0 MeV. This set of data is using the Gaussian multiplicity model only.

The second column shows the χ^2 from the comparison between the data and the fit results. You can compare it with the number of degrees of freedom. The first comment would be to say that the ratio χ^2/N_{df} is very close to the unity except in one case. At an energy threshold cut of 2.5 MeV, run 22348 has a χ^2/N_{df} greater than two. After investigating this run, we found a very compact series of low energy events followed by an empty period of 2.5 minutes at the end of that run. The "shift report" reported a buffer overflow at this end. Consequently, we considered the last 7.3 minutes of the run as unphysical and cut these data. Therefore, a new set of results were created as run 22348x, and the new χ^2/N_{df} becomes closer to 1. Run 22348 will be replaced by 22348x for the rest of this analysis. Finally, all our χ^2/N_{df} ratios are less than 1.2, showing a consistency between our model and the real data.

Because each run presents the same physical conditions (run at centre in salt-D_2O medium), we can merge the results into a single table using this weighted averaging equation [21]:

$$\bar{x} \pm \delta\bar{x} = \frac{\sum_i w_i x_i}{\sum_i w_i} \pm (\sum_i w_i)^{-1/2}, \tag{3.13}$$

where

$$w_i = 1/(\delta x_i)^2. \tag{3.14}$$

For the source fission rates λ, we shifted them to the corresponding value λ' on June 12, 2001, according to the source decay half-lives (see table (3.3)).

We did not include run 20731 to average γ because it is an un-canned situation, which makes the real value different. Also, because we do not know much about the correlation between the excess background λ_{xb} and the source strength, we do not average it.

Considering the results in more detail, let us consider first the parameters τ and λ, i.e. the neutron mean-life and the Cf fission rate. First, it can be seen that τ

E_{th}	γ	ϵ	$\lambda'(s^{-1})$	$\tau(ms)$
2.5	0.200±0.017	0.953±0.005	4.360±0.004	5.281±0.004
3.0	0.196±0.017	0.951±0.005	4.360±0.004	5.281±0.005
3.5	0.175±0.005	0.937±0.004	4.440±0.004	5.281±0.004
4.0	0.151±0.015	0.900±0.004	4.364±0.004	5.283±0.004
4.5	0.121±0.016	0.845±0.005	4.368±0.005	5.291±0.004
5.0	0.116±0.019	0.764±0.006	4.379±0.008	5.293±0.004
5.5	0.095±0.020	0.661±0.007	4.386±0.013	5.294±0.005
6.0	0.122±0.023	0.512±0.007	4.456±0.015	5.295±0.007
6.5	0.162±0.017	0.320±0.002	4.441±0.016	5.309±0.006
7.0	0.126±0.048	0.286±0.005	4.499±0.031	5.287±0.009

Table 3.3: Average of the fits with 5 free parameters. Note that run 20731 is not included to average γ because the un-canned source situation affects the value. Run 22348 is replaced by the corrected 22348x. The λ from each run is shifted to June 12, 2001 value before the averaging, giving the corresponding source strength λ'. In runs 22669 and 22942, γ was enforced to 0 to allow convergence in 3 fits; these γ's do not contribute to the average.

is constant at any energy threshold and for any run. Indeed, we expected that τ was never affected because the thermalised neutrons are only dependent on the cross-sections of the salt-D_2O medium, and not on the source characteristics. And this medium is supposed to be the same since the salt has been mixed with the D_2O. In the table in appendix B, we see that τ changes a little bit at high energy thresholds, but we associate this fluctuation to the poor statistics, since most of the neutron events are cut away.

In addition, the fission rate λ is dependent of the ^{252}Cf and ^{250}Cf life-times. As can be seen, from the different runs, the fission rate decreases with the time as a consequence of the source decay rate (see the dates). But as with τ, λ is constant within each run with the expected statistical uncertainty. To compare directly the decay rates from each run, we must shift each decay rate λ to a same date. Here, λ is shifted back to June 12, 2001 following the ^{250}Cf and ^{252}Cf half-lives and relative

activity weights:

$$\lambda' = \frac{\lambda \times 1.0206}{2^{-d/(365.25\times 2.645)} + 0.0206 \times 2^{-d/(365.25\times 13.08)}}, \tag{3.15}$$

where d is the number of days between the date of a run and June 12, 2001. We can see a small increase of λ' at high energy thresholds; this is probably due to the negative excess background rates λ_{xb} of some runs which move extra background events to the fission rate. Obviously, a negative λ_{xb} is un-physical and we should interpret this rate as $\lambda_{xb} = 0$. To calculate the neutron source rate λ'_n, we multiply λ' by the neutron multiplicity including both Cf neutrons (^{252}Cf and ^{250}Cf multiplicities) and delayed neutrons (3.7630+0.0078). With the value at 2.5 MeV cut, the result is

$$\lambda'_n = 16.44 \pm 0.015 n/s. \tag{3.16}$$

A second observation is that the parameter γ, the probability to detect a prompt γ-cascade as a first fission event, is generally going down with the increase in energy threshold. This is consistent with our prediction, since the energy spectrum is lower than the energy spectrum of the neutron capture and thus the γ-rays detection drop faster than the neutron detection rate. On the other hand, γ is not all the time regular from one run to another, and even irregular from the different threshold of the same run. Our main explanation is that γ is very correlated with ϵ, because of the serious difficulty to distinguish between a γ-ray and a neutron in the first event.

Also, we saw, during the fitting job, the existence of two minimum χ^2. These minima are associated to two different γ values. We believe that the higher γ value is too high to physically make sense. Then, in the case when two minimum χ^2 exist, we chose the convergence including the smallest γ value. Under short runs with bad statistical quality, these two minima might be sometimes indistinguishable, making the fit hard to converge at the right value. This maybe the case for run 22669 for

which nothing can really be learned about γ and ϵ. These two parameters do not satisfy us in this run, and we cannot clearly give a reason for the discrepancies if it is not the short time length of the run. When we compare run 22669 with run 22942, which has the same time length, in this last one, γ and ϵ are more coherent within the run and more consistent with the other runs. We will not include run 22669 in the next results.

3.2.3 The Fit Results with a Fix Decay Rate Parameter

From the 5 free parameters fit, we were very satisfied by the consistency of λ and τ. We were pretty sure that the values obtained for these 2 parameters are very close to the reality. As our second step in the analysis, we fixed λ to a common value within each run. By doing this, the large covariance of λ with γ and ϵ can reduce the statistical fluctuation of γ and ϵ. τ might also be used as a fixed parameter, but the covariance is smaller.

There remains the question of what is the best λ. This parameter is given with tiny differences from each energy thresholds within a run, but obviously, there exists only one real λ from the source. A simple average over the λ's from each energy threshold is not necessarily the best thing to do, because the values are correlated. The correlation occurs because the data used at the high energy thresholds are included into those used at lower energy thresholds. We then decided to fit the data using a series of λ's in the region where the best λ should be. From the 3.0 to 6.0 MeV thresholds, we have calculated χ^2 for each λ. We used only these thresholds because we believe they show the best fits, between lower thresholds where the background noise and γ-rays rate are more significant and higher thresholds where statistics are poorer. Then our "best" λ is defined as that which minimises an average $< \chi^2 >$. $< \chi^2 >$ comes from

E_{th}	γ	ϵ	$\tau(ms)$
2.5	0.209±0.014	0.950±0.004	5.281±0.004
3.0	0.204±0.014	0.948±0.004	5.281±0.004
3.5	0.184±0.013	0.934±0.003	5.280±0.004
4.0	0.149±0.011	0.899±0.003	5.284±0.004
4.5	0.117±0.010	0.847±0.003	5.291±0.004
5.0	0.093±0.009	0.773±0.002	5.293±0.004
5.5	0.074±0.008	0.670±0.002	5.294±0.005
6.0	0.064±0.008	0.544±0.002	5.295±0.005
6.5	0.050±0.008	0.409±0.002	5.309±0.007
7.0	0.029±0.009	0.290±0.002	5.300±0.009

Table 3.4: Average of the Gaussian model fits with λ fixed on each run. Run 22669 is not input in the averages and run 20731 is excluded to average γ.

these calculated χ^2 weighted by the number of events available by the threshold cut, and the 1σ uncertainty $\delta\lambda$ is determined by finding where the $< \chi^2 >$ is increased by unity. Other averaging methods did not change significantly the possible best λ such that our best λ values can be consider as very close to the real λ.

The rest of the work was to remake the fit by enforcing λ with our best estimate. The result are shown in the second part of appendix B. The first set of results comes from the fit using the Gaussian multiplicity distribution whereas the second set is with the hot band distribution. Weighted averaging are also shown in tables (3.4) and (3.5).

As expected, the variations in the parameters γ and ϵ are reduced compared to the previous results with 5 free parameters. But while ϵ and τ are close between our two multiplicity models, γ remains very different. It shows the importance, and our dependence, of finding the right set of multiplicity distribution. Unfortunately, a comparison between the χ^2 of each model does not show that one model provides better fits.

At least, enforcing a λ calculated from intermediate energy threshold data to all

E_{th}	γ	ϵ	$\tau(ms)$
2.5	0.161±0.013	0.961±0.003	5.281±0.004
3.0	0.157±0.012	0.959±0.003	5.281±0.004
3.5	0.139±0.012	0.945±0.003	5.281±0.004
4.0	0.108±0.010	0.910±0.003	5.284±0.004
4.5	0.080±0.009	0.855±0.002	5.291±0.004
5.0	0.061±0.008	0.780±0.002	5.294±0.004
5.5	0.046±0.008	0.676±0.002	5.294±0.005
6.0	0.041±0.007	0.549±0.002	5.296±0.005
6.5	0.031±0.007	0.413±0.002	5.310±0.007
7.0	0.016±0.008	0.293±0.002	5.300±0.009

Table 3.5: Average of the hot fission model fits with λ fixed on each run. Run 22669 is not input in the averages and run 20731 is excluded to average γ.

thresholds helps to decrease the statistical discrepancies of the high energy thresholds, where the poor statistics does not converge as good as lower thresholds to the right λ. Using a better λ should improve the convergence of the other parameters to better values. More discussion about these results are available in [11].

Chapter 4

Other Works with the Time Series Analysis

Even if the Time Series results are consistent and generally agree with what was expected, some checks and new developments still need to be done. The need for a Time Series analysis is ultimately to fix a value for the neutron detection efficiency as accurate as possible. But this accuracy is dependent at different levels on the 4 other fitted parameters, especially the γ factor, and also with our neutron multiplicity knowledge. To try to improve this analysis, we consider further work on three specific aspects: new neutron multiplicity models, the analysis of an AmBe source and a way to measure the prompt γ fraction. Also, we applied the model to some runs at off-centre positions.

4.1 Three Other Neutron Multiplicity Models

The exactitude of the Time Series analysis is directly dependent on the exactitude of the neutron multiplicity distribution. In our analysis, we used two different models

n	Gaussian	Hot fission	Balagna [22]	Wild [23]	Spencer [24]
0	0.00347	0.00346	0.003±0.001	0.0025±0.0004	0.00211±0.00019
1	0.02780	0.02773	0.021±0.005	0.0282±0.0024	0.02467±0.00090
2	0.11782	0.11750	0.140±0.011	0.1199±0.0081	0.12290±0.00125
3	0.26406	0.26335	0.264±0.017	0.2681±0.0278	0.27144±0.00106
4	0.31301	0.31217	0.307±0.020	0.3056±0.0118	0.30763±0.00065
5	0.19624	0.19573	0.191±0.018	0.1951±0.0217	0.18770±0.00087
6	0.06507	0.06514	0.061±0.013	0.0674±0.0158	0.06770±0.00053
7	0.01141	0.01234	0.008±0.007	0.0084±0.0048	0.01406±0.00018
8	0.00106	0.00214	0.005±0.003	0.0045±0.0030	0.00167±0.00005
9	0.00005	0.00040	-0.0006±0.0005	0.0004±0.0015	0.00010±0.00002
10	0.00000	0.00003	N/A	N/A	N/A

Table 4.1: Multiplicity probability table from our 2 previous models and 3 new references.

for the ^{252}Cf, the Gaussian and the Hot-band fission models. For ^{250}Cf we used the Gaussian model based on the ^{252}Cf, but with the ^{250}Cf average neutron distribution. The multiplicity probabilities of each model followed Gaussian distributions. But since our first Time Series work, we have found new experimental values for the multiplicity distribution of ^{252}Cf. The table (4.1) shows these values.

We applied these three new models on run 21023 to compare with the two used in the previous chapter. Run 21023 is used because it is the longest run we have (24 hrs) and it is supposed to provide the best statistics of all available runs. Proceeding with the 5 free parameters fit, and with the usual energy threshold cuts, we get the results shown in tables (4.2), (4.3), (4.4) and (4.5).

An indication that a model's fit seems to be better than another is given by the χ^2/N_{df} ratios. In this case, Wild's and Spencer's multiplicity distribution give slightly better fits at 3.0 and 4.0 MeV cuts than the others. But at 5.0 and 6.0, no distribution makes a significant improvement compared to any other. The Gaussian fit has the

Model	χ^2/N_{df}	γ	ϵ	$\lambda(s^{-1})$	$\tau(ms)$	$\lambda_{xb}(s^{-1})$
Gaussian	792.0/678.0	0.223±0.028	0.937±0.008	4.103±0.006	5.290±0.007	0.519±0.005
Hot-Band	786.1/678.0	0.175±0.024	0.948±0.007	4.099±0.006	5.290±0.007	0.522±0.005
Balagna	792.0/678.0	0.102±0.023	0.987±0.007	4.045±0.007	5.291±0.007	0.570±0.006
Wild	783.0/678.0	0.144±0.022	0.959±0.006	4.090±0.006	5.290±0.007	0.527±0.005
Spencer	783.4/678.0	0.104±0.020	0.973±0.006	4.071±0.006	5.291±0.007	0.543±0.005

Table 4.2: Fits using 5 multiplicity models at 3.0 MeV threshold cut, applied on run 21023 data.

Model	χ^2/N_{df}	γ	ϵ	$\lambda(s^{-1})$	$\tau(ms)$	$\lambda_{xb}(s^{-1})$
Gaussian	761.1/677.9	0.163±0.025	0.892±0.007	4.104±0.007	5.294±0.007	0.141±0.005
Hot-Band	757.1/677.9	0.121±0.022	0.902±0.006	4.099±0.007	5.294±0.007	0.145±0.005
Balagna	760.9/677.9	0.058±0.021	0.938±0.007	4.044±0.008	5.295±0.007	0.190±0.006
Wild	755.4/677.9	0.093±0.020	0.913±0.006	4.090±0.007	5.295±0.007	0.150±0.005
Spencer	755.3/677.9	0.056±0.019	0.926±0.006	4.069±0.007	5.295±0.007	0.166±0.005

Table 4.3: Fits using 5 multiplicity models at 4.0 MeV threshold cut, applied on run 21023 data

worst χ^2/N_{df} for any threshold, and its bad performance can be understood since it is a model only and simply based on the mean multiplicity and the 1σ width of the distribution. By opposition, the four other models add more information from experiments and are expected to better represent the reality.

A look at the parameters shows that τ does not vary between models, showing it is essentially independent of the multiplicity distribution. In the case of λ, ϵ and λ_b, the values are slightly different between models. And the largest fluctuations is with γ. The correlation between these 4 last parameters seems to agree with equation (2.18): since the number of detected events in a run is fixed, if we change the mean neutron multiplicity μ, the 4 free parameters in (2.18) must oppose some variation in their values to keep fixed the total number of detected events. Also, as explained in (3.2.1), the part $\gamma + \mu\epsilon$ is correlated to the short-short peak, λ with the long-short and short-long and λ_b with the long-long one. So any change in μ should induce a change in γ

Model	χ^2/N_{df}	γ	ϵ	$\lambda(s^{-1})$	$\tau(ms)$	$\lambda_{xb}(s^{-1})$
Gaussian	718.9/677.7	0.130±0.030	0.763±0.009	4.118±0.012	5.298±0.007	0.003±0.009
Hot-Band	717.8/677.7	0.087±0.025	0.773±0.008	4.109±0.012	5.298±0.007	0.009±0.008
Balagna	717.7/677.7	0.041±0.023	0.801±0.008	4.058±0.013	5.298±0.007	0.044±0.009
Wild	717.4/677.7	0.061±0.023	0.783±0.008	4.097±0.011	5.298±0.007	0.015±0.008
Spencer	717.9/677.7	0.028±0.022	0.795±0.007	4.075±0.011	5.298±0.007	0.030±0.008

Table 4.4: Fits using 5 multiplicity models at 5.0 MeV threshold cut, applied on run 21023 data

Model	χ^2/N_{df}	γ	ϵ	$\lambda(s^{-1})$	$\tau(ms)$	$\lambda_{xb}(s^{-1})$
Gaussian	728.1/677.7	0.137±0.081	0.521±0.026	4.157±0.053	5.295±0.009	-0.035±0.031
Hot-Band	727.6/677.7	0.084±0.053	0.536±0.018	4.134±0.046	5.295±0.009	-0.022±0.027
Balagna	727.5/677.7	0.055±0.045	0.554±0.016	4.089±0.045	5.295±0.009	-0.001±0.027
Wild	727.3/677.7	0.059±0.045	0.545±0.016	4.117±0.043	5.295±0.009	-0.015±0.026
Spencer	727.7/677.7	0.037±0.040	0.553±0.015	4.097±0.043	5.295±0.009	-0.006±0.026

Table 4.5: Fits using 5 multiplicity models at 6.0 MeV threshold cut, applied on run 21023 data.

and ϵ first since λ and λ_b are well isolated by their respective peaks. And because $\mu\epsilon$ is normally a large value compared to γ, this last must probably vary more than ϵ, if we change μ, to keep the sum $(\gamma + \mu\epsilon)$ as constant as possible. Then it happens that γ varies more with the neutron multiplicity than any other parameter.

Since it is not obvious as to which model is preferred from our comparisons, it is certainly better to use Wild's and Spencer's distributions for further times series analysis: Spencer has the most accurate measurements for each multiplicity channel and Wild has the most recent (1990) of our 5 tested models. The 3 new tested models have also the advantage to show a probability for each possible multiplicity, instead of the two first, based on Gaussian distributions from the mean multiplicity and a mean hot-band multiplicity.

4.2 The Time Series Analysis on an AmBe Source

For the neutron detection efficiency calibration, SNO also used an AmBe source. This source makes a different chronology of the events than the Cf source, and provide a different approach to improve the fit of some parameters. We applied a modified Time Series analysis on two AmBe calibration runs.

4.2.1 The Time Series Model for an AmBe Source

The Am isotopes are essentially α emitters, and as explained in chapter 2, the α decay cannot be directly detected. But with the presence of ^{9}Be, the α's can be captured and the following reaction happens:

$$\alpha + {}^9Be \longrightarrow {}^{13}C^* \longrightarrow {}^{12}C + n + \gamma \tag{4.1}$$

$$\alpha + {}^9Be \longrightarrow {}^{13}C^* \longrightarrow {}^{12}C + n \tag{4.2}$$

where the emission of a 4.44 MeV γ-ray affects how much energy is released into the neutron. Note that the ^{13}C* de-excites by emitting a neutron and not by γ-ray emission. The AmBe source runs are then expected to show sequences of isolated events and pairs. A high correlation can be seen between events from reaction (4.1), when the γ-ray is instantly detected after the nuclear reaction and the neutron capture is also detected after its thermal diffusion. The interval of time between these events, seen as pairs in the chronology of the detected events, have a typical time length equal to τ, the mean life of a neutron.

The Time Series model in the AmBe scenario is a simplification of the Cf model. If γ and ϵ are respectively the probability to detect a γ-ray and the probability to detect a neutron in reaction (4.1), and the rate of this reaction is λ_p, the rate of

detection of correlated events is

$$B = \gamma\epsilon\lambda_p. \tag{4.3}$$

The correlated events can also be detected as single events if one member of the pairs is not detected. Then, the rate of single detections from correlated events is $[\gamma(1-\epsilon)+\epsilon(1-\gamma)]\lambda_p$. We include all other possible single events, such as the neutron from reaction (4.2) and the background, into a total detection rate Λ_b. The total single detection rate is then written as

$$A = (\gamma + \epsilon - 2\gamma\epsilon)\lambda_p + \Lambda_b. \tag{4.4}$$

The total rate of events is $A + 2B$ since B is a pair.

A simple way to connect the AmBe model with the demonstration shown in section 2.2 is to see the similarity with source having only a possible multiplicity of 1. Then, $S^{(1)}(t,t') = S_1^{(1)}(t,t')$ and $S_1^{(1)}(t,t')$ is shown in equation (2.26). It has a direct correspondence between $A + B$ and $\lambda_b + \lambda S^{(1)}(t,t')$. From equation (2.25), the joint survival function for AmBe source is

$$\mathcal{S}(t,t') = [A \ + \ B\,(e^{-t/\tau} + e^{-t'/\tau})]\ e^{-(A+B)(t+t') - B\,\tau[1-\exp(-(t+t')/\tau)]}. \tag{4.5}$$

With this model, 3 free parameters can be fitted: the single event rate A, the pair rate B and the neutron mean-life τ.

4.2.2 The Application on AmBe Data

As for the Cf source, we built a $26X26$ Time Series array. But because the AmBe source has a lower event rate than the Cf source, we shifted the time interval by two rows and two columns compared to the Cf arrays to see greater time intervals. The arrays are then built by this logic:

$$column\ \# \ \ = \ \ 5log_{10}(\Delta t_{before}) - 8, \tag{4.6}$$

E_{th}	χ^2/N_{df}	$A(s^{-1})$	$B(s^{-1})$	$\tau(ms)$
2.0	645.2/628.9	1.580±0.012	1.144±0.008	5.211±0.049
3.0	666.9/631.0	1.515±0.011	1.129±0.008	5.232±0.049
4.0	704.4/630.6	1.666±0.011	0.742±0.007	5.293±0.064
5.0	634.1/615.1	1.826±0.010	0.259±0.005	5.158±0.123

Table 4.6: Fit results on AmBe run 25885 at different energy threshold cuts. The run is 2.44 hrs long. It has 3 free parameters: the single event rate A, the correlated event pair rate B and the neutron mean life τ.

E_{th}	χ^2/N_{df}	$A(s^{-1})$	$B(s^{-1})$	$\tau(ms)$
2.0	696.0/653.7	1.535±0.005	1.120±0.003	5.237±0.022
3.0	674.8/657.0	1.479±0.005	1.109±0.003	5.230±0.022
4.0	633.2/664.4	1.637±0.005	0.753±0.003	5.202±0.027
5.0	621.4/662.0	1.816±0.005	0.264±0.002	5.121±0.053

Table 4.7: Fit results on AmBe run 27574 at different energy threshold cuts. The run is 12.77 hrs long.

$$row\ \# \quad = \quad 5log_{10}(\Delta t_{after}) - 8, \tag{4.7}$$

where the intervals Δt are given in μsec. An example of an array is shown in figure (4.1). We can see three peaks: the front central peak represents the long-long time interval count and depends on the single event rate (the parameter A); the two side peaks are long-short (at left) and short-long (at right) intervals and represent respectively the count of first and last event in correlated event pairs (the parameter B). Obviously, the long-short and short-long peaks are roughly the same size since they are associated to the same number of pairs.

We applied fits on two ROOT files from AmBe calibration runs: SNO_025885_p0.root and SNO_027574_p0.root. These are from older file version than the Cf used files and so they are different in energy normalisation. The results are displayed for different energy threshold cuts in tables (4.6) and (4.7).

The most interesting result is τ. Because the neutron diffusion inside the salt-D_2O

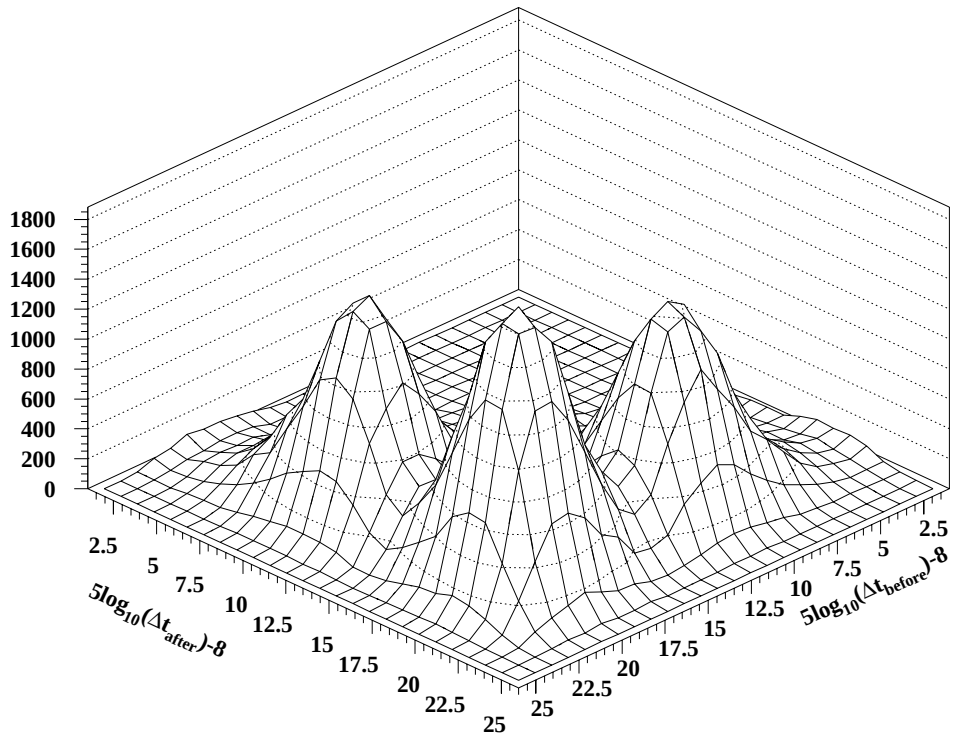

Figure 4.1: Time Series array from AmBe run 27574 at 2.0 MeV threshold cut. The central front peak is the long-long time interval counts, and is proportional to the number of single events. The left peak is the long-short count and the right one, the short-long intervals. They are respectively proportional to the amount of first and last event in correlated event pairs.

is source independent, the neutron mean life must be the same using the AmBe or the Cf source. However, τ is slightly lower than the Cf source results, as summarised into table (4.8). We still believe that neutron mean life is the same independently of the source. So we attribute the difference to an imperfect modeling.

A more complete discussion about the analysis of the AmBe source is in Nickel and Labranche [25].

Source	Model	Parameters	3.0 MeV cut	4.0 MeV cut	5.0 MeV cut
Cf	Gaussian	5 free	5.281±0.005	5.283±0.004	5.293±0.004
Cf	Gaussian	λ fixed	5.281±0.004	5.284±0.004	5.293±0.004
Cf	Hot-Band	λ fixed	5.281±0.004	5.284±0.004	5.294±0.004
AmBe	-	A, B, τ	5.230±0.020	5.215±0.025	5.127±0.048

Table 4.8: Summary of τ from the different models. The averaging are calculated with the weighted averaging equation (3.13). The AmBe results show a lower τ than the Cf results.

4.3 The Prompt γ-Ray Fraction

The most fluctuating parameter is γ by far. Because γ is highly correlated with ϵ, and also significantly correlated with λ and τ, any fluctuation of γ has strong effect on these correlated parameters. And as we saw in our results, γ is the most unstable parameter when we fit. The problem is in the difficulty for the Time Series model to distinguish if first detected fission events are γ-cascades or neutron captures. The time interval distribution between a γ-cascades and the first neutron capture is very close, if not identical, to the time interval distribution between the two first captured neutrons, such that it makes hard to see if the first interval is between a γ-cascade and a neutron or between two neutrons. It might also be possible for the model to find γ by counting the average number of events per fission and subtracting it by the mean neutron multiplicity per fission, but to do this we must already know the neutron detection efficiency, and it is not the case.

4.3.1 First, Second and Last Event Energy Distributions

Thus, we spent some effort to find another method that can better extract γ. The approach we suggest is using the energy spectrums from γ-cascades and from neutrons, which are distinguishable, to differentiate the proportion of γ-cascades and neutrons

into first detected events of fissions. A difference in energy spectrum is expected between the first detected event of a fission and any other subsequent events of a fission, since the detected γ-cascades are exclusively contained in the first events population and the other events are strictly neutrons. Because the time scale difference between the fissions time intervals and the neutron capture time intervals into the same burst is large, it becomes easy to isolate what would be the first detected event of a fission.

We modified the Time Series ROOT reading programme to record the energy of each first, second and last events in a burst. To recognise the first event of a fission burst, we ask for any events having intervals of time greater than 39.8 msec to the previous event and less than 3.98 msec to the next event. When we read the energy of these events, the programme fills a table with energy bins of 0.1 MeV width. The energy of the following event in these bursts is also recorded. The number of counted first and second events is then the same. Finally, we ask for the energy of the final event of each fission burst, the final event being identified as having an interval of time less than 10.0 msec before and more than 39.8 msec after.

The energy spectrum of the second and the last events of fission bursts are supposed to be identical to the neutron energy spectrum measured by the detector as they contain exclusively neutrons. The first events energy spectrum is however a superposition of the γ-ray and the neutron energy spectrums. The key idea is to realise that the second and last event energy distribution must have the same shape as the neutron energy distribution of the first event set. If we multiply a normalisation factor F_n to the counts from the second events, we can renormalise the second event distribution such that it can represent the neutron energy spectrum in the first event spectrum. By maximising a neutron energy spectrum curve under the first event energy spectrum curve, we can find the upper possible fraction of first events that are

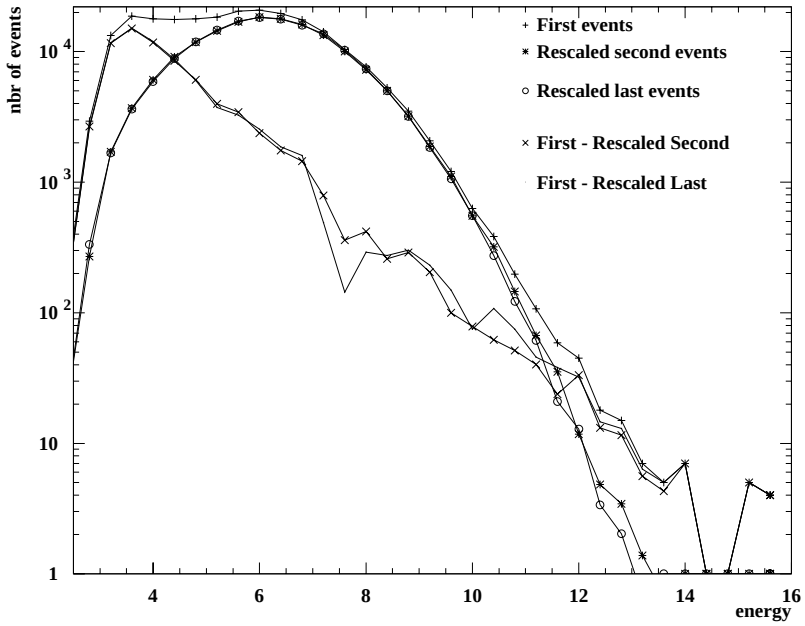

Figure 4.2: First, second and last fission event energy spectrums. The data are from run 21023. The second and last event spectrums are renormalized to fit under the first event spectrum as they represent typical neutron energy spectrums. This normalisation tries to maximise the presence of neutrons in the first events. By subtracting the first event total counts by the renormalized neutron spectrums in each bin, we find the lowest possible γ-ray spectrum, which represents at least $31\% \pm 2\%$ of all first detected fission events. An energy binning of 0.4 MeV was used to cancel as much as possible the PMTs discretisation effect.

neutrons, and consequently the lowest possible prompt γ-ray fraction. Replacing the second event energy distribution by the last event one should give the same result. The figure (4.2) shows the energy distribution above 2.5 MeV of the first, second, and last event and the normalisation when the method is applied to run 21023. The neutron spectrum is maximised under the first event energy spectrum and then a lower limit of γ-ray spectrum is found. The possible normalisation factor must be $F_n \leq 0.69 \pm 0.02$ and then the minimum possible proportion of γ-rays in first detected fission events is $F_\gamma = 31\% \pm 2\%$ ($F_\gamma = 1 - F_n$).

A first comment from the figure (4.2) is that, as expected, the neutron energy spectrum has the same shape using the second or last events. Also, we can realise that neutron captures and γ-cascades have clearly two different energy distributions, where the neutron captures are mostly detected with about 6 or 7 MeV, and the γ-cascades more likely around 4 MeV. But one of the most interesting results from this energy analysis is the presence of very high detector energy response to some γ-cascades. While the detector response for the 8.58 MeV γ-ray emission on capture on the ^{35}Cl is never higher than 13 MeV, some first detected fission events have detector responses that go up to 16 MeV. We attribute these high energetic responses to multiple γ-ray emissions from Cf fissions and detected together as a single event within a same fission.

4.3.2 The γ-Ray Fraction for Different Energy Threshold Cuts

As a next step, we calculated the γ-ray fraction of the first events for different energy threshold. The application of this calculation is that we can afterwords make a correlation between the γ-ray fraction and the Time Series parameter γ. From the first event spectrum, the renormalised neutron spectrum at $F_n = 0.69$, and the resulting γ-ray spectrum obtained in figure (4.2), we plotted the sum of the events for each energy spectra according to the energy threshold cut. By dividing each sum by the sum of first events according to the energy threshold, we get figure (4.3).

We used in figure (4.3) the upper bound normalisation factor $F_n = 0.69$. This factor gives the maximum possible neutron ratio and the minimum possible γ-ray ratio according to what the energy spectrums allow. It is not yet possible to know if the real γ-ray proportion is higher, but the Time Series fit and some other considerations

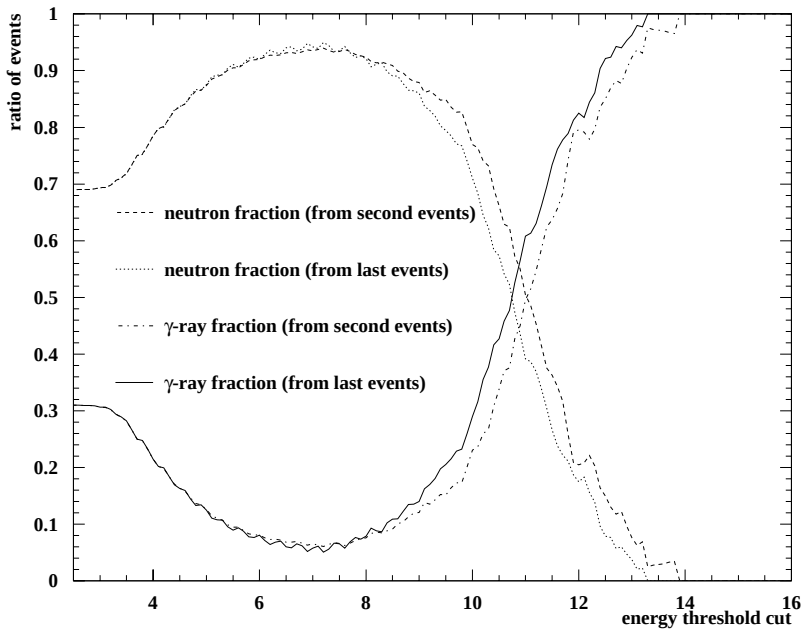

Figure 4.3: Neutron and γ-ray ratios of first detected fission events according to the energy threshold cut. Two sets of ratios are obtained from the second detected events and from the last detected events energy spectrum. The graph shows that at 2.5 MeV energy cut, at least 31% of first detected fission events are γ-rays and that the γ-ray fraction is minimised to 5% if we cut out the events below 7.0 MeV.

tend to estimate the γ-ray fraction close to the maximum normalisation factor bound $F_n \leq 0.69$. On the graph, the γ-ray ratio curves start at 31%, from the ratios of figure (4.3) at 2.5 MeV cut. Then the γ-ray ratio decreases to 5% at 7.2 MeV cut (the minimum in our data is at this threshold cut). This energy threshold cut minimises the presence of γ-rays, but the ratio does not vanish. After, as the threshold increases, the γ-rays rapidly become the dominant first detected fission events. We can then assume that for any energy threshold, it has a contamination of at least 5% of prompt γ-cascade within the first detected fission events.

4.3.3 The Correlation Between the γ-Ray Fraction and the Parameter γ

The γ-ray fraction F_γ in this energy spectrum analysis and the parameter γ from the Time Series analysis are not identical parameters. The difference is in the technique to identify the first detected fission events. To be identified as a first detected event, the event must be detected after more than 39.8 msec of time gap and followed by at least one detected subsequent event within 3.98 msec. The fraction is also correlated to the neutron detection efficiency ϵ since the first detected event population contains detected neutrons and because at least one subsequent neutron must be detected. On the other hand, the Time Series parameter γ is not constrained by any typical time interval checks, and allow a probability to detect the prompt γ-rays within any time intervals before and after, including prompt γ-rays not followed by detected neutrons of the same fission. We can connect these two parameters by an equation.

For a single fission, the probability that a first detected event be a γ-ray is γ. To identify it as a first fission event, it must be preceded by a long interval of time and followed by an event within a short period T. As a unique fission, we can set the interval of time before the first detection to infinity. For a fission producing n neutrons, the probability to identify a γ-ray as first detected event is, using the joint survival equation (2.19) for the prompt γ-ray case, $S^{(1)}_{\gamma ray}(\infty, 0) - S^{(1)}_{\gamma ray}(\infty, T)$. Averaged over the neutron multiplicity fractions f_n, we find

$$P_\gamma = \gamma \sum_{n=0}^{\infty} f_n[1 - (1 - \epsilon + \epsilon e^{-T/\tau})^n]. \tag{4.8}$$

To have a neutron as first detected event, the γ-ray must not be detected: $1 - \gamma$. To be identified as first event, a subsequent neutron must be detected within the interval T. Because we ask an infinite interval of time before the first detection, the case can

be represented with only the survival equation (2.20) for neutrons. As for the γ-ray case, for a fission producing n neutrons, the probability that a neutron is identified as the first detection for that fission is $S^{(1)}_{neutron}(\infty,0) - S^{(1)}_{neutron}(\infty,T)$. Averaged over the multiplicity distribution, we find

$$P_n = (1-\gamma)\sum_{n=0}^{\infty} f_n[1-(1-e^{T/\tau})(1-\epsilon)^n - e^{T/\tau}(1-\epsilon+\epsilon e^{-T/\tau})^n]. \tag{4.9}$$

Combining the two probabilities, we have the probability to identify a first detected event for a fission $P_\gamma + P_n$. Note that $P_\gamma + P_n$ cannot reach unity since the technique does not count a first event for every fission. For example, any fission with less than two detections cannot contribute.

From equations (4.8) and (4.9), the fractions F_γ and F_n can be defined as

$$F_\gamma = P_\gamma/(P_\gamma + P_n), \tag{4.10}$$

$$F_n = P_n/(P_\gamma + P_n), \tag{4.11}$$

where P_γ and P_n depend on γ,ϵ and τ.

Although the exact correlation F_γ and F_n with γ, ϵ and τ requires using the general Time Series model with many fissions, non-fission background and overlapping, the corrections to the relations above should be minor, even neglectable, as long as $\tau \ll (\lambda+\lambda_b)^{-1}$. With $\tau \approx 5.3$ msec and $(\lambda+\lambda_b)^{-1} \approx 220$ msec, we consider sufficiently low the contamination by an independent event into a fission burst. Also, we believe that most corrections should have a proportional effect on both P_γ and P_n and then will not affect the ratios between F_γ and F_n.

The energy spectrum analysis seems to be a very promising approach to improve the discrimination between γ-rays and neutrons. The actual results show a maximum possible fraction of neutron contained into the first detected event. Once we are able to fix the normalisation factor F_n with more certitude, it will be easy to fix some realistic

values for the γ parameter of the Time Series. It also seems that the correlation of F_γ and F_n with γ, ϵ and τ can lead to a new method to find the neutron detection efficiency. A longer analysis of the energy spectrum is in [26].

4.4 The Source at Off-Centre Positions

A limitation of the Time Series analysis is that the neutron diffusion must be contained within the salt-D_2O. The Time Series assumes a simple exponential distribution of time intervals between fissions and neutron captures. Then, if some neutrons diffuse within a medium with a different capture cross section, the distribution in time for captures becomes a more complex function, not developed yet. Referring to figure (2.2) and section (2.1.2), a neglectable fraction of the neutrons diffuses farther than 250 cm around the source. The neutron diffusion should be contained within the salt-D_2O if the source is placed anywhere less than 350 cm from the centre. Thus, we extended the Time Series analysis to some runs where the Cf source positions are within 400 cm from the centre.

A dozen new Cf calibration runs are within 400 cm from the centre. Unfortunately, some runs did not provide good data quality and did not converge with 5 free parameters. Some had excess of short-short counts, as with run 22348 (discussion in section (3.2.2)), which might come from a detector problem. At least, we do not believe it is a physical change relative to centre positions since other off-centre runs fit as the centre ones and show consistent result with what we expected. Lets see in more detail the fits on three typical off-centre runs displayed in table (4.9) and compare them with run at centre 21023. The five free parameter fits are given in tables (4.10), (4.11) and (4.12).

ROOT files	nbr of days since June 12, 2001	radial position (cm)	x (cm)	y (cm)	z (cm)	time length (sec)
SNO_021023_p1.root	89	22	0	-22	0	86402
SNO_025721_p1.root	374	379	-2	-265	-271	14476
SNO_025725_p1.root	375	368	0	260	260	14792
SNO_028527_p1.root	580	327	0	-260	210	7466

Table 4.9: Sample of off-centre runs for Time Series analysis. Cartesian positions (x,y,z) and radial positions are given. The z-axis is the vertical.

In general, all five parameters are consistent. The parameters λ' and τ are very constant at any position while γ and ϵ fluctuate a little bit between runs. But with a more careful look at γ and ϵ, it seems that the differences are more related to the high correlation between γ and ϵ than the position: where ϵ is higher than in some runs, γ is lower, and vice versa. We also selected these runs such that we can check if there are discrepancies due to a chimney at the top of the detector. At the chimney, no PMTs are installed, so the detection efficiency must be lower for events occurring near the chimney. In our sample, the source in run 25725 is at 260 cm above the detector centre and at 271 cm below the centre in run 25721. We do not see significant detection efficiency differences between these two runs. The distance of the source from the centre in these off-centre runs is not enough large to see the asymmetry of the detector. Thus, any run with the source within 400 cm from the centre can be analysed with the actual Time Series model, since no significant amount of neutron diffuses out of the salt-D_2O medium.

Run	χ^2/N_{df}	γ	ϵ	$\lambda'(s^{-1})$	$\tau(ms)$	$\lambda_{xb}(s^{-1})$
21023	792.0/678.0	0.223±0.028	0.937±0.008	4.370±0.007	5.290±0.007	0.519±0.005
25721	621.5/681.0	0.133±0.053	0.965±0.016	4.343±0.016	5.231±0.017	0.534±0.010
25725	676.0/680.9	0.152±0.056	0.960±0.016	4.381±0.016	5.245±0.017	0.515±0.010
28527	645.7/684.0	0.122±0.075	0.974±0.022	4.350±0.023	5.294±0.025	0.441±0.012

Table 4.10: Gaussian model fits on 3 off-centre runs at 3.0 MeV threshold cut. Run 21023 gives a comparison with the results at centre. The parameter λ' is λ shifted to June 12, 2001 activity.

Run	χ^2/N_{df}	γ	ϵ	$\lambda'(s^{-1})$	$\tau(ms)$	$\lambda_{xb}(s^{-1})$
21023	761.1/677.9	0.164±0.025	0.892±0.007	4.371±0.007	5.294±0.007	0.141±0.005
25721	631.7/681.6	0.059±0.045	0.921±0.014	4.339±0.018	5.243±0.017	0.136±0.009
25725	682.3/681.5	0.046±0.043	0.921±0.013	4.369±0.017	5.249±0.017	0.133±0.009
28527	721.0/685.2	0.114±0.079	0.910±0.024	4.358±0.027	5.304±0.025	0.103±0.012

Table 4.11: Gaussian model fits on 3 off-centre runs and run 21023 at 4.0 MeV threshold cut.

Run	χ^2/N_{df}	γ	ϵ	$\lambda'(s^{-1})$	$\tau(ms)$	$\lambda_{xb}(s^{-1})$
21023	718.9/677.7	0.130±0.030	0.763±0.009	4.385±0.013	5.298±0.007	0.003±0.009
25721	625.7/681.8	0.025±0.051	0.789±0.017	4.337±0.029	5.248±0.018	0.035±0.016
25725	656.7/681.7	0.028±0.052	0.776±0.017	4.361±0.031	5.249±0.018	0.034±0.017
28527	750.7/686.2	0.235±0.238	0.726±0.071	4.408±0.068	5.325±0.028	-0.010±0.032

Table 4.12: Gaussian model fits on 3 off-centre runs and run 21023 at 5.0 MeV threshold cut.

Chapter 5

The Multiplicity Analysis

Before the development of the Time Series Analysis, we concentrated our work on the Multiplicity Analysis. This former method was used for the neutron detection efficiency calibration during the Pure-D_2O Phase of SNO [7]. And we were expecting to also use it for the Salt-D_2O Phase. Here we summarise the theory and some of the analysis done for the Salt-D_2O Phase. We must understand that the work is incomplete since we have stopped it when the Time Series Analysis became more promising.

5.1 The Neutron Multiplicity Function

The Multiplicity Analysis consists in correlating the probability to detect d neutrons in a time interval Δt with the neutron detection efficiency ϵ and the fission rate λ. In other words, a function $P(d)$, the probability to detect d neutrons in a time interval Δt, was developed, and it is dependent of the average fission rate, the detection efficiency, and the ^{252}Cf multiplicity. We do not have to talk again about the source since it is the same as for the Time Series Analysis.

Within a day, the quantity of ^{252}Cf in the source is a very large number in comparison with the number of fissions occurring. Lets define λ as the average number of fissions per small interval of time T. Because the ^{252}Cf fissions occur in time independently from each other, the probability f_N that N fissions occur within T is the Poisson distribution

$$f_N = \frac{\lambda^N e^{-\lambda}}{N!}. \tag{5.1}$$

If we sum f_N over all possible N fissions, we obviously get unity. But for the next calculations, it is more useful to keep it as a summation $f = f_0 + f_1 + \cdots$ and write

$$f = e^{-\lambda} + \sum_{N=1}^{\infty} \frac{\lambda^N e^{-\lambda}}{N!}. \tag{5.2}$$

Since we have ruled the distribution in number of fissions per interval of time, we must calculate the same thing now with the neutrons, in correlation with the number of fissions per interval of time. A ^{252}Cf fission emits a random number of neutrons. As explained in section (3.1.3), the distribution in number of neutrons per fission can be modeled by a Gaussian function. Then the probability for a fission n to emit r_n neutrons is

$$P_1(r_n) = \frac{e^{-\frac{(r_n-\mu)^2}{2\sigma^2}}}{\sqrt{\pi 2\sigma^2}}, \tag{5.3}$$

where μ is the mean neutron multiplicity for a fission and σ is the standard width of neutron multiplicities in the Gaussian distribution. In an interval of time, we have a total number of neutrons $r = r_1 + r_2 + \cdots + r_N$ from the N fissions that occur. The probability from N fissions to produce r neutrons is $P_N(r) = \sum P(r_1) \cdot P(r_2) \cdots P(r_N)$ where the sum is over all combinations of $r_1 \cdots r_N$, whose total is r. The result is

$$P_N(r) = \frac{e^{-\frac{(r-N\mu)^2}{2N\sigma^2}}}{\sqrt{2\pi N\sigma^2}}. \tag{5.4}$$

To generalise (5.4) to all possible number of fissions N, we must combine the two probabilities f_N and P_N as $P(r) = \sum_N f_N P_N$. For the probability to produce r

neutrons in an interval of time where the average possible number of fission is λ, we find

$$P(r) = e^{-\lambda}\delta_{r,0} + \sum_{N=1}^{\infty} \frac{e^{-\frac{(r-N\mu)^2}{2N\sigma^2}}}{\sqrt{2\pi N}\sigma} \cdot \frac{\lambda^N e^{-\lambda}}{N!}. \tag{5.5}$$

If r neutrons are produced, we do not necessarily detect all of them. Here we must include the neutron detection efficiency ϵ. For r neutrons, the probability to detect all of them is ϵ^r. On the other hand, to detect none of them is $(1-\epsilon)^r$. In the general case, the probability to detect d of the r produced neutron is $\epsilon^r(1-\epsilon)^{r-d}$ multiplied by a binomial coefficient:

$$P_r(d) = \frac{r!\epsilon^d(1-\epsilon)^{r-d}}{d!(r-d)!}. \tag{5.6}$$

If we do not know how many r neutron are produced in an interval, the probability to detect d neutron is the sum of $P_r(d)$ over all possible r combined with a weight $P(r)$, as $\sum_r P_r(d)P(r)$. The result gives the probability $P(d)$ to detect d neutron within a interval of time, namely

$$P(d) = e^{-\lambda}\delta_{d,0} + \sum_{N=1}^{\infty}\sum_{r=d}^{\infty} \frac{r!\epsilon^d(1-\epsilon)^{r-d}}{d!(r-d)!} \cdot \frac{e^{-\frac{(r-N\mu)^2}{2N\sigma^2}}}{\sqrt{2\pi N}\sigma} \cdot \frac{\lambda^N e^{-\lambda}}{N!}, \tag{5.7}$$

The equation (5.7) is called the Multiplicity Function. The function depends on 4 parameters: the average number of fission per interval of time λ, the neutron detection efficiency ϵ, the mean neutron multiplicity per fission μ and the neutron multiplicity standard deviation σ. While for the experiment μ and σ are well known, we fit the function with the experimental data to find ϵ and λ.

5.2 Data Analysis with the Multiplicity Function

The data used in this analysis are the same ROOT files as with the Time Series, but with energy response normalisation version available in August 2002. To treat

the data, a programme divides the whole run into 2 sec intervals. In each interval, it counts how many events are detected above a certain energy threshold. Then, for each interval with d neutrons, it increments by a unity the $(d+1)$th value of a vector. At the end, the vector is saved into a file for the fitting of (5.7).

We use Minuit [20] to fit the Multiplicity function (5.7) with the data vector. Because there are many low or zero counts in the data vector, it is important to use as χ^2 the Poisson formula (3.7), also explained in [19]. Minuit outputs a χ^2, the degree of freedom, and the best ϵ and λ with their statistical uncertainties. Figure (5.1) shows a fit example.

The Multiplicity function is independent of the neutron diffusion time and so it can be applied to any source position inside the AV. Fittings were done for most Cf calibration runs available in December 2001. The Appendix C shows the neutron detection efficiency for each run according to the radial position of the source.

It is interesting to see that near the AV, the neutron detection efficiency drops. As described in [5], the efficiency for a given source radial position s gives

$$\epsilon(s) = \epsilon_0 \left[1 - \frac{R\sinh(s/l)}{s\sinh(R_e/l)} \left[\cosh(\frac{R_e - R}{l}) + \frac{l}{R}\sinh(\frac{R_e - R}{l})\right]\right]. \qquad (5.8)$$

where R is the fiducial radius, R_e the effective fiducial radius, l the neutron diffusion length and ϵ_0 the detection efficiency for an infinite volume of salt-D_2O. For the Salt Phase, ϵ_0 is identical to the $\epsilon(s = 0)$ since the neutron diffusion is entirely contained within the salt-D_2O medium. The detector has $R = 600$ cm and $R_e = 616$ cm and the salt-D_2O has $l \approx 33.7$ cm. The curve shown in each graph of appendix C is the plot of (5.8), after an average of centre run efficiencies to get ϵ_0. The table (5.1) gives the efficiencies at the centre for the different energy threshold cuts.

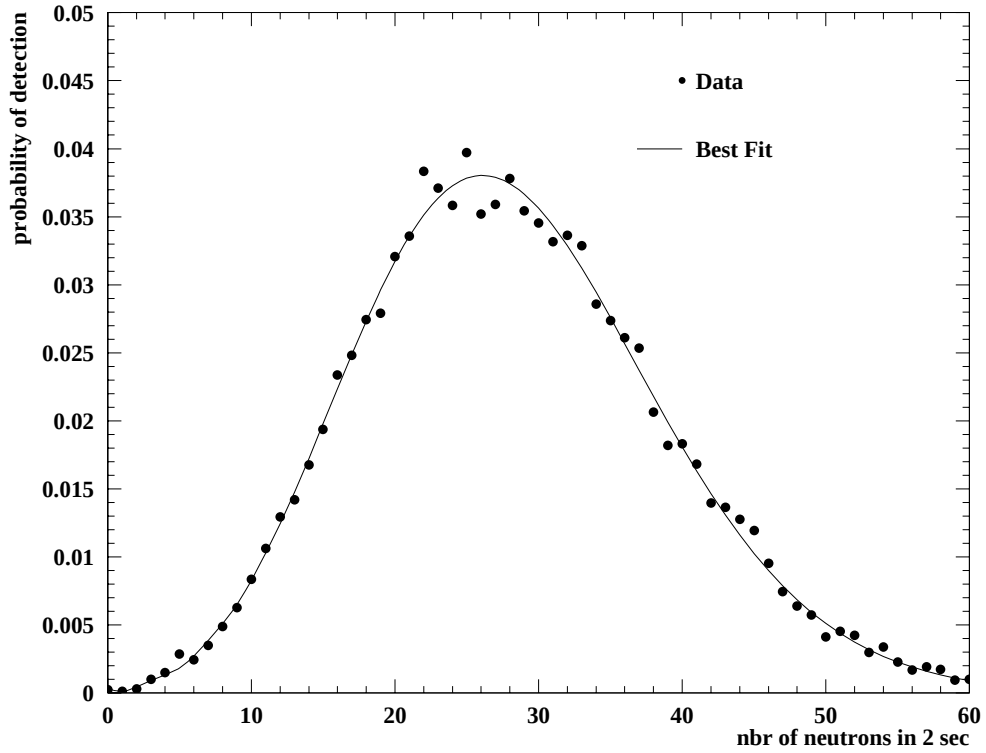

Figure 5.1: Distribution of the number of neutrons per 2 sec time interval. The Multiplicity function is fitted onto this distribution to find the best λ and ϵ. The above graph is from run 21023 with a 4.0 MeV energy threshold cut. The χ^2 vs the number of degree of freedom for this fit is $\chi^2/N_{df} = 0.9641$.

5.3 Discussion About the Multiplicity Analysis

The Multiplicity Analysis is characterised as a method which neglects the background activity and does not consider the diffusion time of neutrons. To neglect the background activity was valid during the Pure-D_2O Phase since a radial cut was applied around the source to reduce efficiently the background count. But in the salt-D_2O, the neutrons are concentrated in the same volume where the source background is, so the radial cut cannot be applied without significantly reducing the count of neutrons. Thus, it is not possible to distinguish neutron events and prompt γ-rays and other

E_{th}	ϵ_0
2.0	0.885±0.044
3.0	0.915±0.046
4.0	0.898±0.042
5.0	0.725±0.037
6.0	0.461±0.029
7.0	0.209±0.017

Table 5.1: Detection efficiency at centre for different energy threshold cuts. All runs within 1.0 m from the centre are used to calculate the averages. The energy threshold values here do not directly correspond with the threshold values of the Time Series because the energy responses are not from the same energy calibration updates.

backgrounds.

When a fission occurs, the Multiplicity model assumes that every event from it are detected at the same instant. But in fact, the neutrons survive with a mean life τ before their capture. It means that for a fission occurring a bit before the limit between two time interval bins, the model cannot represent correctly the situation if some neutrons are detected in the first bin and others in the next bin. But with a 2 sec binning and $\tau \approx 0.005$ sec, bursts overlapping two bins are rare. On the other hand, to not consider the diffusion time makes the model compatible with runs at any source position.

Chapter 6

Conclusion

6.1 Conclusion of the Time Series Analysis

To fix the efficiency of SNO to detect the neutral current reaction from ^{8}B solar neutrinos, a neutron source made with californium is used. Based on the intrinsic characteristics of the californium fissions, the survival function $\mathcal{S}(t, t')$ has been developed to describe the chronology of detected events when the Cf source is put into the SNO Detector. It is then possible to extract the neutron detection efficiency ϵ, the probability γ to detect prompt fission γ-rays, the source fission rate λ, the neutron capture mean-life within the salt-D_2O medium τ and the residual background rate λ_b coming from the source and the detector.

The intervals of time between detected events in Cf calibration runs were arrayed such that the array can be fitted with the survival function. The 5 parameters were found from 8 runs with source at the centre and with different energy threshold cuts. The method converges efficiently and with great consistency for the parameters λ and τ. With the 5 free parameters fits over all the events above 2.5 MeV, we find on

average

$$\begin{aligned} \lambda' &= 4.360 \pm 0.004(\text{stat.})\ \text{sec}^{-1} \\ \tau &= 5.281 \pm 0.004(\text{stat.})\ \mu\text{sec} \\ \lambda'_n &= 16.44 \pm 0.015(\text{stat.})\ \text{neutron/sec.} \end{aligned}$$

where λ' is the fission rate of the source at June 12, 2001 and λ'_n is the neutron rate at the same date.

On the other hand, ϵ and γ are very correlated and then they fluctuate more than the other parameters. To improve the method for finding the best ϵ and γ, we enforced λ to be constant. The main improvement was to make the parameters at high energy threshold more consistent with those at lower threshold.

As recent developments, we found new references about neutron multiplicity and we suggest hereafter to use the results from Wild [23] or Spencer [24] since they are closer to the real multiplicity distribution than the simple Gaussian distribution. We analysed also the data from an AmBe source to find τ as a little bit lower than the results from the Cf although it is supposed to be the same. We added results from some off-centre runs which are far enough from the AV to not allow the neutron to diffuse out of the salt-D_2O. These off-centre runs are consistent with those at centre. To improve the differentiation between prompt γ-rays and neutrons, we extracted their energy spectrums and found the fraction of first fission events which are not neutrons.

The Time Series only show the neutron detection efficiency at the centre. But these results can be already useful for SNO since other analysis provide the variation of efficiency with the radial position of the source. Our results can then be used to evaluate the efficiency for an infinite volume of D_2O, ϵ_0. And ϵ_0 can be used to

normalise properly the equation (5.8). Since other techniques need the Cf source strength to normalise the efficiency properly, the Time Series can also provide them with an independent measurement.

6.2 What Is Next?

At the moment we write this thesis, the Time Series analysis is in development since only 7 months. Obviously, a multitude of things need to be checked or improved.

The energy spectra provide an opportunity to improve the differentiation between the γ-rays and neutrons, since they do not have the same spectrum. With the relations correlating F_n, F_γ, γ and ϵ, it is now possible to enforce γ to a known value. Since the primary goal of this analysis is to find ϵ with as much accuracy as possible, to impose γ to its right value seems an essential step.

We also have to find why τ is different between the AmBe and the Cf runs. This discrepancy is maybe a problem in our models. A hypothesis would be that the AmBe source has a stronger neutron absorbance than the Cf one, meaning that neutrons can be captured by crossing the source after diffusing in the salt-D_2O.

To analyse the source near the AV, the Time Series model needs to consider the neutron diffusion into different mediums at the same time. In this situation, some neutrons escape into the H_2O, where the capture cross section is higher, and their life-times are very reduced compared to that within the D_2O. The model will probably have new free parameters such as the fractions of neutron captured in the D_2O, the H_2O and maybe the AV, and different neutron mean life for each medium. Unfortunatly, more free parameters will certainly make the fitting convergence harder.

And to achieve this analysis, we obviously need to investigate the systematic

uncertainties. But now, the Time Series analysis have proven how a careful study of the Cf fission can lead to accurate measurements of the source strength and the neutron detection efficiency of SNO's detector.

Bibliography

[1] J.N. Bahcall *et al. Solar Neutrinos, The First Thirty Years.* Westview Press, (2002).

[2] A. B. McDonald, J. R. Klein, and D. L. Wark. Solving the solar neutrino problem. *Sci. Am.*, 288N4:22–31, 2003.

[3] Q. R. Ahmad et al. Measurement of the charged current interactions produced by ^{8}B solar neutrinos at the Sudbury Neutrino Observatory. *Phys. Rev. Lett.*, 87:071301, 2001.

[4] Q. R. Ahmad et al. Direct evidence for neutrino flavor transformation from neutral-current interactions in the Sudbury Neutrino Observatory. *Phys. Rev. Lett.*, 89:011301, 2002.

[5] M.Kos. Neutron detection efficiency during the salt phase of SNO. (2003).

[6] M.Dragowsky and A.Hime. Neutron response and efficiency for the pure D_2O phase in SNO. (2002).

[7] J.J.Simpson. The strength of the strong Cf-source and the efficiency for detecting neutrons. *SNO-STR-2001-002*, (2001).

[8] M.Fowler and J.B.Wilhelmy. Preparation of acrylic encapsulated radioactive calibration sources for SNO. *SNO-STR-99-016*, (1999).

[9] R.B. Firestone. *Table of Isotopes, Eighth Edition.* Wiley-Interscience, (1996).

[10] A.C. Wahl. . *Atomic Data and Nuclear Data Tables* ***39***, (1988).

[11] H. Labranche, J. Law, and B. G. Nickel. Time series analysis of SNO ^{252}Cf source. (May 15, 2003).

[12] B.G.Nickel. private comunication. 9905026.

[13] E. Segrè. *Nuclei and particles, 2^{nd} edition.* W.A.Benjamin, Inc., Reading, Massachusetts, (1977).

[14] B.G .Nickel and H. Labranche. Efficiency of neutron detection from ^{252}Cf source time series. (February 12, 2003).

[15] CERN. http://root.cern.ch/.

[16] M.R.Dragowsky, M.M.Fowler, A.Hime, G.G.Miller, and J.B.Wilhelmy. Measurement of the ^{252}Cf acrylic source standard. (2001).

[17] G.M.Ter-Akopian et al. . *Phy. Rev. C* ***85***, 1146, (1997).

[18] S.-C.Wu et al. . *Phy. Rev. C* ***62***, 41601, (2000).

[19] S. Baker and R.D. Cousins. . *Nucl. Instrum. Methods* ***221***, 437, (1984).

[20] CERN. wwwinfo.cern.ch/asdoc/minuit/minmain.html.

[21] *Physical Review D, Particles and Fields, vol. 66, Third Series, Part I.* The American Physical Society, (2001).

[22] J.P. Balagna *et al.* Prompt neutrons from the spontaneous fission of ^{257}Fm. *IAEA-SM-174/77.*

[23] J.F. Wild *et al.* Prompt neutron emission from the spontaneaous fission of ^{260}Md. *Phys. Rev. C* ***41***, 640-646, (1990).

[24] R.R. Spencer *et al.* A measurement of the average number of prompt neutrons from spontaneous fission of californium-252. *Nucl. Sc. and Engineering* ***80***, 603, (1982).

[25] B. G. Nickel and H. Labranche. Time series analysis of the AmBe source. (May 20, 2003).

[26] H. Labranche, J. Law, and B. G. Nickel. Time series analysis of SNO ^{252}Cf source. (June 25, 2003).

Appendix A

The Times Series Arrays

A.1 The Programme to Make Arrays

```
{
//Write the energy threshold here (in MeV):
Float_t e_threshold = 6.0 ;

//Some initialisations for the whole analysis:
char name[19];
Int_t tot_negdt,tot_lardt;
tot_negdt=tot_lardt=0;
char threshold[0];
sprintf(threshold,"%d",e_threshold*10);

//read the list of files to analyse:
ifstream filename ("files");
while (! filename.eof() ){

  //read one file:
  filename.getline (name,19);

  //make the name of the root file to read:
  char rootfile[42];
  strcpy(rootfile,"/data5/cf_root/");
  strcat(rootfile, name);
  printf("Read data from: %s\n", rootfile);

  //make the name of the file where to save data:
  char resultfile[60];
  char run_num[11];
  strncpy(run_num,name,10);
```

```
//strcpy(resultfile,"/helioshome/hlabranc/expdist/scraptests/");
strcpy(resultfile,"/data5/cf_2dts/");
strcat(resultfile, threshold);
strcat(resultfile,"MeVts/");
strcat(resultfile, run_num);
strcat(resultfile, "-");
strcat(resultfile, threshold);
strcat(resultfile, ".ts");
printf("Results will be saved in: %s\n", resultfile);

//Initialisation of the variables
Int_t ntot,n,i,j,k,k_old,l,m,first,negdt,lardt,gooddt;
Float_t e_init,e_final,xs,ys,zs,rr;
Double_t t1_init,t2_init,t3_init,t1_first,t2_first;
Double_t t1_final,t2_final,t3_final;
Double_t logdt,dt1,dt2,dt3,dt,dt_run;
Double_t negdtlist[10],lardtlist[10];
//26 X 26 =352 bins of data:
Int_t casier[26][26];

//All integers reset to zero:
ntot=n=i=j=k=k_old=l=m=first=negdt=lardt=gooddt=0;
for (i=0;i<10;i++) negdtlist[i]=lardtlist[i]=0;
for (i=0;i<26;i++) {
  for (j=0;j<26;j++) casier[i][j] = 0;
}

//extract the data from the root file:
TFile *f1 = new TFile(rootfile);
QTree *T1 = (QTree*)f1->Get("T");
QEvent *event1 = new QEvent();
QFit *fita = new QFit();
ntot = (Int_t)T1->GetEntries();
printf("Total nbr of events: %d\n",ntot);
T1->SetEventAddress(event1);

//one loop per event:
while (n<ntot){
  if (n % 50000 == 0) printf("%d analysed events\n",n);

  //Identification of the first event time (in sec):
  if (first == 0){
    T1->GetEvent(n);
    t1_init = (event1.GetJulianDate());
    t2_init = (event1.GetUT1());
    t3_init = (event1.GetUT2());
    t1_first = t1_init;
    t2_first = t2_init;
    printf("First time found\n");
```

```
      first = 1;
      n = n+1;
    }

    //Identification of the next event time (in sec):
    T1->GetEvent(n);
    t1_final = (event1.GetJulianDate());
    t2_final = (event1.GetUT1());
    t3_final = (event1.GetUT2());
    fita = event1->GetFitByIndex(10);

    if (fita != NULL) {
      //Get the energy and position:
      QRSP *R3 = event1->GetRSPByIndex(10);
      e_final = R3.GetEnergy();
      xs=fita->GetX();
      ys=fita->GetY();
      zs=fita->GetZ();
      rr = sqrt(pow(xs,2) + pow(ys,2) + pow(zs,2));

      //Energy threshold, radial cut & time interval checks:
      if (e_final > e_threshold && rr < 600.0) {
dt1=(t1_final-t1_init)*8.64e10;
dt2=(t2_final-t2_init)*1.0e6;
dt3=(t3_final-t3_init)/1000.0;
dt = dt1 + dt2 + dt3;
if (dt<0.0) { //some events are not sort properly!
  negdt = negdt + 1;
  tot_negdt = tot_negdt + 1;
  printf("!!!!!negative dt: %f sec\n",dt);
  negdtlist[negdt-1] = dt;
}
else if (dt>1.0e7) { //some ROOT files show big gaps!
  lardt = lardt + 1;
  tot_lardt = tot_lardt + 1;
  printf("!!!!!large dt: %f sec\n",dt);
  lardtlist[lardt-1] = dt;
}
//when all the conditions are satisfied, add to the array:
else {
  logdt = log10(dt)*5.0-6.0;
  k=floor(logdt);
  if (k<1) k=0;     //border rows and columns
  if (k>=25) k=25;     //are special cases
  casier[k][k_old] = casier[k][k_old] + 1;
  gooddt = gooddt + 1;
}
t1_init = t1_final;
t2_init = t2_final;
```

```
t3_init = t3_final;
k_old=k;
      }
    }

    n=n+1;
    k = 0;
  }

  //calculate the time for whole run and make some corrections on:
  dt_run = (t1_final-t1_first)*8.64e4+(t2_final-t2_first);
  for(l=0;l<negdt;l++){
    if (negdtlist[l]<-1.0e7) dt_run = dt_run - negdtlist[l]/1.0e6;
  }
  for(m=0;m<lardt;m++) dt_run = dt_run - lardtlist[m]/1.0e6;

  f1->Close();

  //Save data on a file:
  FILE *fp;
  fp = fopen(resultfile,"w");
  fprintf(fp,"%f\n ",dt_run);
  for (l=0;l<26;l++){
    for (m=0;m<26;m++) fprintf(fp,"%d ",casier[l][m]);
    fprintf(fp,"\n ");
  }
  fprintf(fp,"\nnbr of good dt (in the array):%d\n",gooddt);
  fprintf(fp,"nbr of negative dt:%d\n",negdt);
  for(l=0;l<negdt;l++) fprintf(fp,"%f sec\n",negdtlist[l]/1.0e6);
  fprintf(fp,"nbr of dt > 10sec :%d\n",lardt);
  for(m=0;m<lardt;m++) fprintf(fp,"%f sec\n",lardtlist[m]/1.0e6);
  fclose(fp);

  //Print a brief of the data:
  printf("%d analysed events\n",n);
  printf("%d good events\n",gooddt);
  printf("time of the run: %f sec\n", dt_run);
}
printf("***** a total of %d bad dt\n", tot_negdt+tot_lardt);
}
```

A.2 A Sample of Array

This array is from run 22348 with a 2.5 MeV threshold cut. The first value is the run time length. The matrix is the time interval array. A log at the end show which

interval was excluded to make the array.

```
46676.737169
 359 31 67 86 116 187 215 363 469 497 515 346 278 127 85 85 157 213 271 368 385 375 274 105 28 1
 45 15 33 31 66 82 140 242 258 304 295 228 167 81 46 66 76 121 152 207 256 211 132 67 9 0
 51 32 47 62 88 172 254 299 429 457 470 406 241 126 74 109 140 182 282 316 369 323 213 99 21 0
 89 39 70 107 162 243 355 503 641 811 725 627 387 203 140 164 193 283 398 478 568 470 347 147 25 5
 115 66 123 165 246 402 567 802 985 1140 1118 928 571 283 216 181 308 430 587 770 859 793 487 239 42 3
 179 107 183 242 398 586 844 1238 1524 1655 1756 1451 865 470 299 320 460 658 911 1217 1329 1254 757 339 73 1
 309 152 271 369 606 887 1241 1763 2220 2636 2600 2079 1350 733 449 484 704 985 1377 1681 1995 1640 1122 470 101 7
 408 216 364 532 828 1254 1809 2556 3344 3899 3826 3153 1968 1078 617 655 933 1348 1875 2405 2710 2432 1554 640 164 10
 522 298 464 719 1067 1678 2511 3408 4510 5240 5309 4474 2796 1466 880 910 1281 1762 2509 3237 3477 3179 2110 844 189 13
 646 370 560 916 1392 2006 2954 4373 5609 6723 6904 5753 3762 1989 1083 1052 1546 2140 2918 3790 4211 3847 2556 1069 199 16
 686 436 623 993 1562 2412 3540 4973 6510 7815 8070 6881 4633 2312 1244 1187 1593 2210 3101 3909 4331 3942 2593 1073 234 15
 692 376 621 1042 1498 2389 3523 4862 6496 7920 8411 7457 5286 2612 1260 993 1339 1843 2721 3335 3704 3355 2174 902 177 16
 556 327 506 827 1203 1896 2662 4049 5286 6809 7665 6838 4954 2677 1194 766 919 1290 1811 2293 2592 2238 1495 593 138 11
 348 215 362 552 800 1240 1901 2726 3796 4811 5538 5530 4048 2203 939 500 518 684 978 1256 1401 1296 757 366 73 6
 212 123 162 269 465 684 1069 1468 2144 2757 3374 3482 2909 1848 830 411 260 365 551 634 708 664 425 140 40 2
 85 53 93 138 222 332 460 731 1104 1391 1839 2100 1905 1486 912 388 209 234 304 382 440 444 262 117 17 2
 56 48 58 85 121 213 318 485 714 1021 1444 1816 1925 1691 1093 539 231 255 356 427 472 404 278 125 26 4
 64 34 64 101 179 242 404 647 971 1322 1742 2233 2435 2210 1451 742 344 322 470 591 606 578 397 170 31 0
 95 62 99 150 229 368 565 796 1311 1818 2425 3092 3435 3133 2115 957 461 490 668 856 875 841 500 195 39 3
 144 80 112 216 295 454 710 1076 1597 2279 3174 3995 4216 3903 2644 1274 615 592 795 1042 1031 1091 695 252 47 7
 124 90 141 215 328 483 829 1134 1771 2532 3463 4166 4925 4285 3001 1385 722 664 935 1106 1330 1204 734 300 58 11
 119 84 140 181 275 462 669 1064 1555 2278 3116 4027 4361 4015 2804 1258 579 677 794 1064 1137 1103 659 274 52 3
 61 45 68 124 195 292 455 679 1062 1527 2026 2667 2756 2561 1725 783 421 415 535 659 784 685 460 167 54 3
 37 26 24 52 70 126 187 277 436 602 882 1020 1189 1109 737 359 159 154 231 248 274 314 184 75 15 2
 6 5 6 6 15 22 46 64 99 131 177 233 213 228 147 72 33 30 46 59 85 66 43 20 3 0
 0 0 1 0 0 4 3 0 12 9 13 22 20 14 11 10 4 3 2 6 7 1 1 1 0 0

nbr of good dt (in the array):735482
nbr of negative dt:3
-1.892637 sec
-3.752495 sec
-1.812981 sec
nbr of dt > 10sec :1
148.262831 sec
```

Appendix B

The Fit results

B.1 The Fit Results with 5 Free Parameters

Run 20731, Day 48 (July 30, 2001), time length = 7.7639 hrs, M = 3.76286

E_{th}	χ^2/N_{df}	γ	ϵ	$\lambda(s^{-1})$	$\tau(ms)$	$\lambda_{xb}(s^{-1})$
2.5	728.3/643.3	0.277(65)	0.975(19)	4.210(13)	5.277(13)	2.853(14)
3.0	720.3/647.4	0.278(65)	0.968(19)	4.210(13)	5.277(13)	2.632(13)
3.5	765.6/662.7	0.225(53)	0.950(15)	4.208(12)	5.271(12)	1.819(12)
4.0	754.9/671.0	0.185(47)	0.915(14)	4.209(13)	5.267(12)	1.093(11)
4.5	693.1/673.7	0.178(52)	0.848(16)	4.219(16)	5.277(12)	0.553(12)
5.0	687.1/674.6	0.182(70)	0.751(22)	4.246(25)	5.290(12)	0.251(18)
5.5	693.5/674.8	0.191(144)	0.637(45)	4.276(57)	5.285(14)	0.106(38)
6.0	676.1/675.3	0.240(157)	0.490(44)	4.333(36)	5.284(15)	0.000(20)
6.5	628.0/677.3	0.170(322)	0.368(93)	4.345(118)	5.300(18)	-0.027(50)
7.0	685.2/679.8	0.125(107)	0.256(30)	4.362(78)	5.285(25)	-0.033(32)

Run 21023, Day 89 (Sept. 9, 2001), time length = 24.0006 hrs M = 3.76273

E_{th}	χ^2/N_{df}	γ	ϵ	$\lambda(s^{-1})$	$\tau(ms)$	$\lambda_{xb}(s^{-1})$
2.5	788.7/673.0	0.230(29)	0.937(8)	4.104(6)	5.290(7)	0.564(5)
3.0	792.0/673.0	0.223(28)	0.937(8)	4.103(6)	5.290(7)	0.519(5)
3.5	779.2/673.0	0.195(26)	0.930(7)	4.101(6)	5.289(7)	0.356(5)
4.0	761.1/672.9	0.164(25)	0.892(7)	4.104(7)	5.294(7)	0.141(5)
4.5	746.6/672.8	0.146(26)	0.835(8)	4.110(9)	5.300(7)	0.045(6)
5.0	718.9/672.7	0.130(30)	0.763(9)	4.118(12)	5.298(7)	0.003(9)
5.5	663.9/672.6	0.131(45)	0.647(15)	4.133(24)	5.312(8)	-0.020(16)
6.0	728.1/672.7	0.137(77)	0.521(25)	4.157(50)	5.295(9)	-0.035(29)
6.5	730.8/673.2	0.172(18)	0.370(5)	4.215(19)	5.326(11)	-0.057(11)
7.0	646.0/675.0	0.126(86)	0.258(24)	4.240(48)	5.321(14)	-0.050(19)

Run 22348, Day 158 (Nov. 17, 2001), time length = 12.9658 hrs M = 3.76252

E_{th}	χ^2/N_{df}	γ	ϵ	$\lambda(s^{-1})$	$\tau(ms)$	$\lambda_{xb}(s^{-1})$
2.5	1538.1/673.7	0.232(40)	0.949(12)	3.884(8)	5.269(9)	0.848(7)
3.0	795.5/673.8	0.189(34)	0.957(10)	3.878(8)	5.268(9)	0.672(6)
3.5	691.6/673.8	0.156(30)	0.944(9)	3.873(8)	5.267(9)	0.366(6)
4.0	700.7/673.8	0.164(34)	0.897(10)	3.884(9)	5.274(9)	0.149(6)
4.5	695.7/673.7	0.148(37)	0.838(11)	3.888(11)	5.283(9)	0.053(8)
5.0	725.7/673.6	0.128(42)	0.758(13)	3.903(17)	5.288(10)	0.008(12)
5.5	729.0/673.5	0.050(37)	0.681(13)	3.873(24)	5.271(11)	0.013(17)
6.0	689.3/673.9	0.034(47)	0.551(17)	3.856(49)	5.296(12)	0.020(30)
6.5	670.6/675.1	0.091(118)	0.394(41)	3.927(130)	5.307(15)	-0.019(61)
7.0	735.6/677.5	0.130(108)	0.260(30)	3.991(57)	5.306(20)	-0.037(23)

Run 22348x, Day 158 (Nov. 17, 2001), time length = 12.8847 hrs, M = 3.76252

E_{th}	χ^2/N_{df}	γ	ϵ	$\lambda(s^{-1})$	$\tau(ms)$	$\lambda_{xb}(s^{-1})$
2.5	783.3/673.7	0.187(33)	0.961(10)	3.882(8)	5.268(9)	0.854(7)
3.0	746.5/673.8	0.178(32)	0.960(9)	3.880(8)	5.267(9)	0.673(6)
3.5	694.0/673.9	0.155(30)	0.945(9)	3.877(8)	5.267(9)	0.366(6)
4.0	695.7/673.9	0.163(33)	0.897(10)	3.890(9)	5.273(9)	0.147(6)
4.5	684.1/673.8	0.148(36)	0.838(11)	3.895(11)	5.283(9)	0.050(8)
5.0	714.6/673.6	0.129(41)	0.758(13)	3.909(16)	5.287(10)	0.006(12)
5.5	677.6/673.5	0.052(37)	0.680(13)	3.880(24)	5.270(11)	0.011(17)
6.0	676.1/673.9	0.037(49)	0.550(18)	3.863(50)	5.294(12)	0.018(31)
6.5	662.7/675.1	0.101(99)	0.391(34)	3.941(101)	5.305(15)	-0.025(48)
7.0	735.6/677.5	0.130(116)	0.260(33)	3.996(59)	5.305(20)	-0.038(24)

Run 22349, Day 159 (Nov. 18, 2001), time length = 10.7672 hrs, M = 3.76252

E_{th}	χ^2/N_{df}	γ	ϵ	$\lambda(s^{-1})$	$\tau(ms)$	$\lambda_{xb}(s^{-1})$
2.5	720.3/673.8	0.176(35)	0.965(10)	3.894(9)	5.278(10)	0.859(7)
3.0	725.5/674.0	0.174(35)	0.961(10)	3.895(9)	5.278(10)	0.679(7)
3.5	716.8/674.2	0.160(34)	0.943(10)	3.897(9)	5.278(10)	0.364(7)
4.0	712.1/674.3	0.119(31)	0.911(9)	3.898(9)	5.281(10)	0.153(7)
4.5	686.8/674.2	0.067(29)	0.863(9)	3.895(11)	5.282(10)	0.063(8)
5.0	699.6/674.0	0.088(38)	0.772(12)	3.901(17)	5.289(11)	0.023(12)
5.5	692.9/674.0	0.091(49)	0.668(16)	3.915(28)	5.281(12)	-0.001(20)
6.0	672.5/674.4	0.225(32)	0.489(9)	4.002(18)	5.303(13)	-0.055(11)
6.5	721.8/675.9	0.156(164)	0.372(49)	4.011(81)	5.286(16)	-0.047(36)
7.0	728.3/678.3	0.124(140)	0.262(40)	3.972(78)	5.241(21)	-0.009(29)

Run 22669, Day 190 (Dec. 19, 2001), time length = 1.0119 hrs, M = 3.76242

E_{th}	χ^2/N_{df}	γ	ϵ	$\lambda(s^{-1})$	$\tau(ms)$	$\lambda_{xb}(s^{-1})$
2.5	588.3/669.6	0.478(722)	0.872(195)	3.818(32)	5.277(30)	0.649(22)
3.0	597.6/671.1	0.479(256)	0.868(69)	3.819(25)	5.281(30)	0.523(17)
3.5	591.6/673.2	0.388(456)	0.876(126)	3.816(40)	5.273(32)	0.299(30)
4.0	625.0/675.0	0.278(222)	0.858(64)	3.820(39)	5.263(32)	0.099(28)
4.5	600.5/676.8	0.107(113)	0.846(35)	3.791(38)	5.250(33)	0.057(27)
5.0	640.5/679.3	0.190(212)	0.744(65)	3.820(65)	5.242(35)	0.005(46)
5.5	648.4/683.1	0.012(113)	0.686(40)	3.756(80)	5.241(38)	0.038(56)
6.0	686.1/686.5	0.259(433)	0.477(117)	3.929(64)	5.190(41)	-0.068(38)
6.5	651.6/688.9	0.009(211)	0.426(84)	3.693(370)	5.178(53)	0.056(188)
7.0	721.5/685.8	0	0.298(8)	3.717(162)	5.144(70)	0.025(76)

Run 22942, Day 217 (Jan. 15, 2002), time length = 1.0072 hrs, M = 3.76233

E_{th}	χ^2/N_{df}	γ	ϵ	$\lambda(s^{-1})$	$\tau(ms)$	$\lambda_{xb}(s^{-1})$
2.5	631.9/672.3	0.275(186)	0.920(53)	3.724(31)	5.261(33)	0.543(25)
3.0	611.8/673.1	0.247(161)	0.926(46)	3.722(30)	5.258(33)	0.469(23)
3.5	626.6/674.6	0.187(126)	0.927(37)	3.718(29)	5.259(33)	0.291(21)
4.0	623.1/676.3	0.214(159)	0.871(47)	3.728(35)	5.283(33)	0.090(25)
4.5	591.3/677.9	0.143(132)	0.835(40)	3.728(40)	5.281(34)	0.025(29)
5.0	642.8/680.7	0.048(108)	0.776(35)	3.714(51)	5.286(36)	0.000(37)
5.5	674.2/684.0	-0.056(85)	0.705(31)	3.657(69)	5.294(39)	0.043(49)
6.0	738.6/687.0	-0.163(65)	0.619(27)	3.521(97)	5.264(45)	0.124(65)
6.5	723.1/689.0	0	0.415(3)	3.713(27)	5.266(52)	0.000(0)
7.0	673.9/684.6	0	0.284(8)	3.893(182)	5.199(72)	-0.058(81)

Run 25707, Day 373 (June 20, 2002), time length = 2.0011, M = 3.76180

E_{th}	χ^2/N_{df}	γ	ϵ	$\lambda(s^{-1})$	$\tau(ms)$	$\lambda_{xb}(s^{-1})$
2.5	721.8/676.3	0.198(93)	0.961(27)	3.380(18)	5.333(25)	0.672(15)
3.0	720.6/676.9	0.214(99)	0.952(29)	3.382(19)	5.336(25)	0.539(15)
3.5	709.8/677.8	0.177(88)	0.940(26)	3.386(19)	5.335(24)	0.287(14)
4.0	686.4/678.5	0.094(71)	0.916(21)	3.378(19)	5.324(24)	0.113(14)
4.5	703.5/679.3	0.083(75)	0.863(23)	3.377(24)	5.333(25)	0.048(17)
5.0	745.3/680.4	0.099(97)	0.772(31)	3.396(36)	5.343(26)	0.004(26)
5.5	686.3/681.6	0.241(301)	0.618(89)	3.450(70)	5.348(28)	-0.043(45)
6.0	736.3/683.3	0.246(202)	0.491(56)	3.449(44)	5.371(32)	-0.028(27)
6.5	712.1/685.7	0.089(220)	0.399(76)	3.362(214)	5.440(41)	0.026(103)
7.0	741.0/686.2	0.124(152)	0.259(43)	3.522(124)	5.521(55)	-0.037(53)

Run 28535, Day 581 (Jan. 14, 2003), time length = 8.0056, M = 3.76102

E_{th}	χ^2/N_{df}	γ	ϵ	$\lambda(s^{-1})$	$\tau(ms)$	$\lambda_{xb}(s^{-1})$
2.5	705.7/673.7	0.188(49)	0.945(14)	2.894(9)	5.273(13)	0.409(7)
3.0	702.9/673.7	0.180(47)	0.947(14)	2.893(8)	5.274(13)	0.385(7)
3.5	728.9/673.6	0.174(47)	0.929(14)	2.896(9)	5.278(13)	0.245(6)
4.0	722.0/673.7	0.165(49)	0.893(15)	2.900(10)	5.278(13)	0.104(7)
4.5	726.1/673.7	0.165(58)	0.826(18)	2.907(13)	5.296(13)	0.024(9)
5.0	708.5/673.7	0.127(59)	0.762(19)	2.906(17)	5.293(14)	0.002(12)
5.5	726.2/673.9	0.168(45)	0.635(14)	2.933(17)	5.299(15)	-0.024(11)
6.0	702.7/674.9	0.107(109)	0.529(37)	2.923(61)	5.294(17)	-0.023(36)
6.5	640.0/677.4	0.012(83)	0.423(33)	2.857(111)	5.289(21)	0.012(56)
7.0	679.2/680.5	0.122(196)	0.257(56)	3.071(82)	5.287(27)	-0.074(30)

B.2 The Fit Results with a Fix Decay Rate Parameter

B.2.1 With the Gaussian Multiplicity Model

Run 20731, Day 48 (July 30, 2001),
time length = 7.7639 hrs, λ = 4.2146(-152/+155)

E_{th}	χ^2/N_{df}	γ	ϵ	$\tau(ms)$	$\lambda_{xb}(s^{-1})$
2.5	728.5/644.3	0.2929(552)	0.9697(147)	5.2765(126)	2.8489(96)
3.0	720.4/648.4	0.2917(548)	0.9640(146)	5.2773(125)	2.6285(93)
3.5	765.9/663.6	0.2434(448)	0.9442(120)	5.2710(122)	1.8141(82)
4.0	755.2/672.0	0.1990(375)	0.9105(101)	5.2665(119)	1.0886(72)
4.5	693.2/674.7	0.1679(327)	0.8516(88)	5.2771(120)	0.5560(63)
5.0	689.1/675.6	0.1165(263)	0.7720(71)	5.2889(124)	0.2720(59)
5.5	696.0/675.8	0.0852(226)	0.6726(61)	5.2817(133)	0.1462(57)
6.0	679.2/676.4	0.0605(205)	0.5485(56)	5.2812(151)	0.0681(58)
6.5	628.4/678.3	0.0457(209)	0.4093(58)	5.2987(187)	0.0336(66)
7.0	685.9/680.8	0.0369(243)	0.2862(68)	5.2858(249)	0.0187(86)

Run 21023, Day 89 (Sept. 9, 2001),
time length = 24.0006 hrs λ = 4.1055(-75/ +86)

E_{th}	χ^2/N_{df}	γ	ϵ	$\tau(ms)$	$\lambda_{xb}(s^{-1})$
2.5	788.7/674.0	0.2333(234)	0.9354(62)	5.2899(65)	0.5630(34)
3.0	792.2/674.0	0.2287(229)	0.9347(61)	5.2898(65)	0.5175(34)
3.5	779.7/674.0	0.2051(210)	0.9264(56)	5.2888(65)	0.3532(31)
4.0	761.2/673.9	0.1667(183)	0.8916(49)	5.2941(65)	0.1402(29)
4.5	746.9/673.8	0.1354(163)	0.8389(44)	5.3003(67)	0.0478(29)
5.0	719.9/673.7	0.1056(143)	0.7707(39)	5.2969(70)	0.0109(30)
5.5	665.5/673.6	0.0883(130)	0.6611(35)	5.3111(76)	-0.0020(30)
6.0	729.4/673.7	0.0746(125)	0.5425(34)	5.2934(86)	-0.0040(32)
6.5	732.0/674.2	0.0567(129)	0.4085(35)	5.3242(107)	-0.0062(37)
7.0	647.0/676.0	0.0377(140)	0.2873(39)	5.3212(143)	-0.0029(48)

Run 22348x, Day 158 (Nov. 17, 2001),
time length = 12.8847 hrs, λ = 3.8848(-102/+102)

E_{th}	χ^2/N_{df}	γ	ϵ	$\tau(ms)$	$\lambda_{xb}(s^{-1})$
2.5	783.4/674.7	0.1938(291)	0.9588(78)	5.2680(92)	0.8524(50)
3.0	746.8/674.8	0.1887(283)	0.9562(76)	5.2670(91)	0.6709(47)
3.5	695.0/674.9	0.1724(265)	0.9385(71)	5.2663(90)	0.3615(42)
4.0	696.0/674.9	0.1518(245)	0.9012(66)	5.2736(90)	0.1496(38)
4.5	685.0/674.8	0.1246(221)	0.8461(60)	5.2829(93)	0.0561(38)
5.0	716.9/674.6	0.0826(187)	0.7738(51)	5.2862(98)	0.0217(39)
5.5	677.6/674.5	0.0582(164)	0.6782(45)	5.2704(105)	0.0080(40)
6.0	676.3/674.9	0.0585(163)	0.5426(44)	5.2954(121)	0.0048(42)
6.5	662.8/676.1	0.0555(179)	0.4070(49)	5.3043(149)	0.0021(49)
7.0	736.2/678.5	0.0457(211)	0.2880(59)	5.3046(197)	0.0004(64)

Run 22349, Day 159 (Nov. 18, 2001),
time length = 10.7672 hrs, λ = 3.8975(-104/+116)

E_{th}	χ^2/N_{df}	γ	ϵ	$\tau(ms)$	$\lambda_{xb}(s^{-1})$
2.5	720.4/674.8	0.1827(307)	0.9626(82)	5.2779(101)	0.8575(54)
3.0	725.5/675.0	0.1788(300)	0.9598(80)	5.2779(100)	0.6778(51)
3.5	716.8/675.2	0.1607(280)	0.9425(75)	5.2785(98)	0.3638(45)
4.0	712.1/675.3	0.1171(243)	0.9114(66)	5.2807(99)	0.1536(42)
4.5	686.8/675.2	0.0725(210)	0.8609(57)	5.2817(102)	0.0610(42)
5.0	699.7/675.0	0.0817(204)	0.7746(55)	5.2887(107)	0.0258(43)
5.5	693.3/675.0	0.0651(183)	0.6768(50)	5.2800(115)	0.0108(44)
6.0	675.1/675.4	0.0605(179)	0.5424(49)	5.3000(132)	0.0048(46)
6.5	722.4/676.9	0.0464(184)	0.4095(51)	5.2847(162)	0.0057(53)
7.0	728.4/679.3	0.0605(275)	0.2824(76)	5.2405(213)	0.0165(72)

Run 22942, Day 217 (Jan. 15, 2002),
time length = 1.0072 hrs, λ = 3.7193(-350/+418)

E_{th}	χ^2/N_{df}	γ	ϵ	$\tau(ms)$	$\lambda_{xb}(s^{-1})$
2.5	632.0/673.4	0.2582(1309)	0.9257(350)	5.2617(331)	0.5461(160)
3.0	611.8/674.1	0.2372(1203)	0.9290(322)	5.2587(329)	0.4704(155)
3.5	626.6/675.6	0.1907(1018)	0.9252(273)	5.2587(326)	0.2903(142)
4.0	623.1/677.4	0.1862(988)	0.8796(265)	5.2835(331)	0.0957(133)
4.5	591.3/678.9	0.1210(792)	0.8418(214)	5.2811(339)	0.0308(132)
5.0	642.8/681.7	0.0574(630)	0.7725(171)	5.2867(357)	-0.0031(136)
5.5	674.9/684.9	0.0162(524)	0.6782(143)	5.2977(388)	0.0009(141)
6.0	741.3/688.1	-0.0310(422)	0.5632(116)	5.2737(441)	-0.0030(147)
6.5	722.8/689.9	-0.0242(416)	0.4214(117)	5.2555(544)	-0.0090(165)
7.0	673.8/685.4	-0.0439(371)	0.3044(108)	5.1969(720)	0.0064(202)

Run 25707, Day 373 (June 20, 2002),
time length = 2.0011, λ = 3.3841(-224/+241)

E_{th}	χ^2/N_{df}	γ	ϵ	$\tau(ms)$	$\lambda_{xb}(s^{-1})$
2.5	721.8/677.3	0.2095(816)	0.9574(219)	5.3321(247)	0.6691(113)
3.0	720.6/677.9	0.2196(838)	0.9505(224)	5.3353(246)	0.5378(107)
3.5	709.8/678.8	0.1732(713)	0.9416(191)	5.3349(243)	0.2874(95)
4.0	686.5/679.5	0.1066(582)	0.9121(157)	5.3233(244)	0.1105(87)
4.5	703.6/680.3	0.0983(554)	0.8578(150)	5.3331(251)	0.0440(89)
5.0	745.4/681.4	0.0732(491)	0.7807(133)	5.3422(264)	0.0123(92)
5.5	687.3/682.6	0.0820(478)	0.6697(129)	5.3451(285)	0.0002(94)
6.0	737.1/684.3	0.1087(562)	0.5353(152)	5.3719(326)	0.0094(99)
6.5	712.1/686.7	0.1146(804)	0.3900(218)	5.4400(409)	0.0153(120)
7.0	741.3/687.2	0.0318(493)	0.2914(138)	5.5227(551)	0.0128(147)

Run 28535, Day 581 (Jan. 14, 2003),
time length = 8.0056, λ = 2.8986(-114/+112)

E_{th}	χ^2/N_{df}	γ	ϵ	$\tau(ms)$	$\lambda_{xb}(s^{-1})$
2.5	706.0/674.7	0.2042(425)	0.9399(114)	5.2727(129)	0.4065(48)
3.0	703.4/674.7	0.1993(418)	0.9402(112)	5.2736(129)	0.3814(47)
3.5	729.0/674.6	0.1839(394)	0.9262(106)	5.2776(128)	0.2438(44)
4.0	722.0/674.7	0.1598(361)	0.8950(97)	5.2776(129)	0.1049(41)
4.5	726.6/674.7	0.1357(327)	0.8355(88)	5.2960(133)	0.0300(41)
5.0	708.6/674.7	0.1067(289)	0.7690(78)	5.2926(139)	0.0072(42)
5.5	727.6/674.9	0.0855(258)	0.6622(70)	5.2966(151)	-0.0016(43)
6.0	702.8/675.9	0.0688(244)	0.5426(66)	5.2928(170)	-0.0084(45)
6.5	640.1/678.4	0.0449(238)	0.4097(66)	5.2905(210)	-0.0084(52)
7.0	679.4/681.5	0.0017(200)	0.3003(57)	5.2855(277)	-0.0129(64)

B.2.2 With the Hot-Band Multiplicity Model

Run 20731, Day 48 (July 30, 2001),
time length = 7.7639 hrs, λ = 4.2091(-144/+151)

E_{th}	χ^2/N_{df}	γ	ϵ	$\tau(ms)$	$\lambda_{xb}(s^{-1})$
2.5	727.3/644.3	0.2292(448)	0.9848(119)	5.2765(126)	2.8535(96)
3.0	719.5/648.4	0.2282(444)	0.9791(118)	5.2772(125)	2.6331(93)
3.5	764.6/663.6	0.1880(381)	0.9572(102)	5.2710(122)	1.8186(82)
4.0	753.8/672.0	0.1501(330)	0.9218(88)	5.2666(119)	1.0930(72)
4.5	691.9/674.7	0.1249(293)	0.8615(79)	5.2774(120)	0.5602(63)
5.0	687.5/675.6	0.0818(242)	0.7799(65)	5.2894(124)	0.2760(59)
5.5	694.8/675.8	0.0562(209)	0.6791(57)	5.2823(133)	0.1497(57)
6.0	678.3/676.4	0.0370(189)	0.5538(51)	5.2818(151)	0.0707(58)
6.5	628.2/678.3	0.0267(191)	0.4136(53)	5.2992(187)	0.0351(66)
7.0	685.6/680.8	0.0220(216)	0.2897(61)	5.2861(249)	0.0193(85)

Run 21023, Day 89 (Sept. 9, 2001),
time length = 24.0006 hrs λ = 4.1003(-84/ +71)

E_{th}	χ^2/N_{df}	γ	ϵ	$\tau(ms)$	$\lambda_{xb}(s^{-1})$
2.5	782.8/674.0	0.1816(202)	0.9474(54)	5.2903(65)	0.5669(34)
3.0	786.2/674.0	0.1775(199)	0.9466(53)	5.2902(65)	0.5215(33)
3.5	773.7/674.0	0.1566(185)	0.9376(49)	5.2891(65)	0.3572(31)
4.0	757.1/673.9	0.1230(165)	0.9015(44)	5.2943(65)	0.1442(29)
4.5	743.9/673.8	0.0965(148)	0.8477(40)	5.3006(67)	0.0518(29)
5.0	718.3/673.7	0.0717(132)	0.7784(36)	5.2973(70)	0.0148(30)
5.5	663.9/673.6	0.0594(120)	0.6676(32)	5.3116(77)	0.0012(31)
6.0	728.2/673.7	0.0499(114)	0.5481(31)	5.2940(86)	-0.0016(32)
6.5	731.3/674.2	0.0367(116)	0.4131(32)	5.3247(107)	-0.0048(37)
7.0	646.6/676.0	0.0226(125)	0.2908(35)	5.3215(143)	-0.0024(47)

Run 22348x, Day 158 (Nov. 17, 2001),
time length = 12.8847 hrs, λ = 3.8803(-105/ +94)

E_{th}	χ^2/N_{df}	γ	ϵ	$\tau(ms)$	$\lambda_{xb}(s^{-1})$
2.5	781.3/674.7	0.1470(259)	0.9694(69)	5.2683(92)	0.8559(50)
3.0	744.6/674.8	0.1425(253)	0.9666(68)	5.2672(91)	0.6743(47)
3.5	693.2/674.9	0.1277(239)	0.9486(64)	5.2665(90)	0.3650(41)
4.0	694.7/674.9	0.1107(223)	0.9104(60)	5.2739(90)	0.1531(38)
4.5	683.4/674.8	0.0876(203)	0.8544(55)	5.2832(93)	0.0597(38)
5.0	715.5/674.6	0.0514(174)	0.7806(47)	5.2866(98)	0.0251(40)
5.5	677.4/674.5	0.0315(154)	0.6840(42)	5.2708(105)	0.0110(40)
6.0	676.5/674.9	0.0355(150)	0.5477(41)	5.2960(121)	0.0069(42)
6.5	662.8/676.1	0.0359(161)	0.4115(44)	5.3049(149)	0.0032(48)
7.0	736.0/678.5	0.0298(185)	0.2917(52)	5.3050(197)	0.0008(63)

Run 22349, Day 159 (Nov. 18, 2001),
time length = 10.7672 hrs, λ = 3.8931(-105/+109)

E_{th}	χ^2/N_{df}	γ	ϵ	$\tau(ms)$	$\lambda_{xb}(s^{-1})$
2.5	720.0/674.8	0.1372(276)	0.9728(74)	5.2781(100)	0.8609(54)
3.0	725.3/675.0	0.1339(270)	0.9699(72)	5.2781(99)	0.6812(51)
3.5	716.7/675.2	0.1179(254)	0.9520(68)	5.2787(98)	0.3672(45)
4.0	712.3/675.3	0.0785(225)	0.9199(61)	5.2809(99)	0.1570(41)
4.5	687.1/675.2	0.0384(197)	0.8683(53)	5.2817(102)	0.0645(41)
5.0	699.9/675.0	0.0503(190)	0.7814(51)	5.2890(107)	0.0292(43)
5.5	692.7/675.0	0.0382(172)	0.6827(47)	5.2805(115)	0.0136(44)
6.0	674.1/675.4	0.0377(166)	0.5474(45)	5.3007(133)	0.0068(46)
6.5	722.0/676.9	0.0277(168)	0.4137(46)	5.2852(162)	0.0068(53)
7.0	728.3/679.3	0.0426(231)	0.2867(64)	5.2408(213)	0.0166(71)

Run 22942, Day 217 (Jan. 15, 2002),
time length = 1.0072 hrs, λ = 3.7146(-329/+405)

E_{th}	χ^2/N_{df}	γ	ϵ	$\tau(ms)$	$\lambda_{xb}(s^{-1})$
2.5	631.9/673.3	0.2037(1103)	0.9385(295)	5.2622(331)	0.5497(159)
3.0	611.8/674.1	0.1853(1035)	0.9411(277)	5.2591(329)	0.4739(154)
3.5	626.3/675.6	0.1443(906)	0.9358(243)	5.2591(326)	0.2939(141)
4.0	623.0/677.4	0.1414(879)	0.8898(236)	5.2839(331)	0.0993(132)
4.5	591.3/678.9	0.0834(728)	0.8503(196)	5.2814(339)	0.0345(132)
5.0	642.8/681.7	0.0266(592)	0.7792(160)	5.2868(357)	0.0004(136)
5.5	674.9/684.9	-0.0088(497)	0.6836(135)	5.2979(388)	0.0041(142)
6.0	741.4/688.1	-0.0499(404)	0.5672(112)	5.2738(441)	-0.0005(147)
6.5	722.8/689.9	-0.0387(397)	0.4245(111)	5.2557(544)	-0.0075(165)
7.0	673.8/685.4	-0.0535(357)	0.3065(104)	5.1970(720)	0.0073(201)

Run 25707, Day 373 (June 20, 2002),
time length = 2.0011, λ = 3.3803(-217/+237)

E_{th}	χ^2/N_{df}	γ	ϵ	$\tau(ms)$	$\lambda_{xb}(s^{-1})$
2.5	720.9/677.2	0.1618(722)	0.9683(193)	5.3323(247)	0.6721(112)
3.0	719.7/677.9	0.1713(736)	0.9615(197)	5.3357(245)	0.5408(107)
3.5	708.8/678.8	0.1303(645)	0.9512(173)	5.3354(242)	0.2903(94)
4.0	685.9/679.5	0.0688(540)	0.9204(146)	5.3234(244)	0.1135(87)
4.5	703.1/680.3	0.0626(515)	0.8657(139)	5.3332(251)	0.0471(88)
5.0	745.2/681.4	0.0424(460)	0.7874(125)	5.3425(264)	0.0152(92)
5.5	686.9/682.6	0.0546(444)	0.6757(120)	5.3458(285)	0.0026(94)
6.0	736.7/684.3	0.0820(499)	0.5413(135)	5.3728(326)	0.0109(99)
6.5	712.0/686.7	0.0866(632)	0.3967(172)	5.4405(410)	0.0159(118)
7.0	741.2/687.2	0.0177(445)	0.2947(125)	5.5231(552)	0.0132(145)

Run 28535, Day 581 (Jan. 14, 2003),
time length = 8.0056, λ = 2.8951(-107/+112)

E_{th}	χ^2/N_{df}	γ	ϵ	$\tau(ms)$	$\lambda_{xb}(s^{-1})$
2.5	705.9/674.7	0.1558(375)	0.9510(100)	5.2728(129)	0.4092(47)
3.0	703.2/674.7	0.1514(370)	0.9512(99)	5.2737(128)	0.3841(47)
3.5	729.0/674.6	0.1382(352)	0.9366(95)	5.2777(128)	0.2465(44)
4.0	722.0/674.7	0.1176(327)	0.9046(88)	5.2779(129)	0.1077(41)
4.5	726.2/674.7	0.0978(299)	0.8441(81)	5.2963(133)	0.0327(41)
5.0	708.3/674.7	0.0733(266)	0.7765(72)	5.2930(139)	0.0098(42)
5.5	726.9/674.9	0.0574(239)	0.6685(65)	5.2972(151)	0.0006(43)
6.0	702.7/675.9	0.0451(224)	0.5480(61)	5.2934(171)	-0.0068(45)
6.5	640.1/678.4	0.0262(217)	0.4139(60)	5.2910(210)	-0.0075(51)
7.0	679.4/681.5	-0.0103(188)	0.3030(54)	5.2858(277)	-0.0124(63)

Appendix C

The Neutron Detection Efficiencies from the Multiplicity Analysis

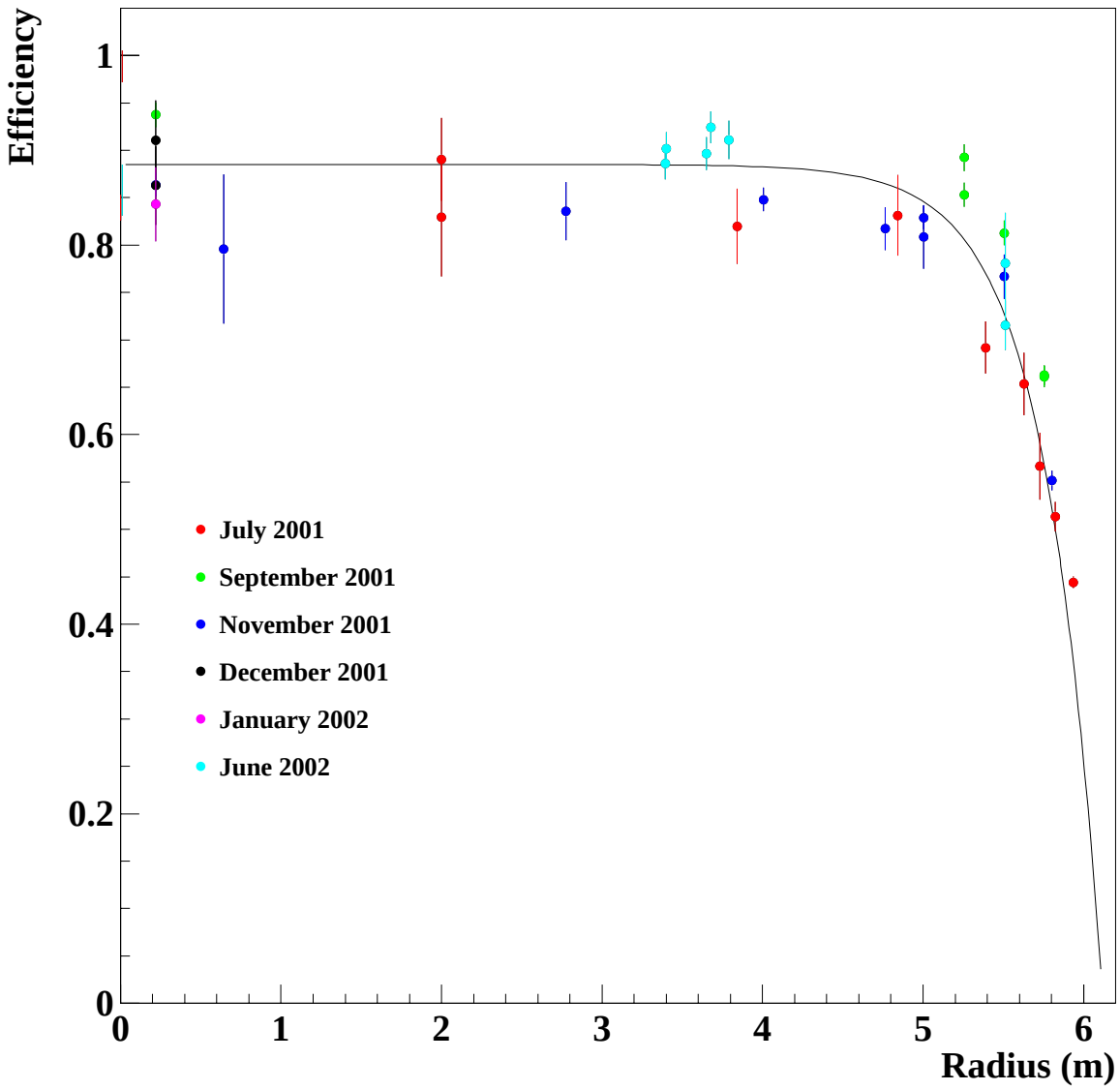

Figure C.1: Efficiency vs source radial position with 2.0 MeV energy threshold cut. Efficiency at center is $\epsilon_0 = 0.885 \pm 0.044$.

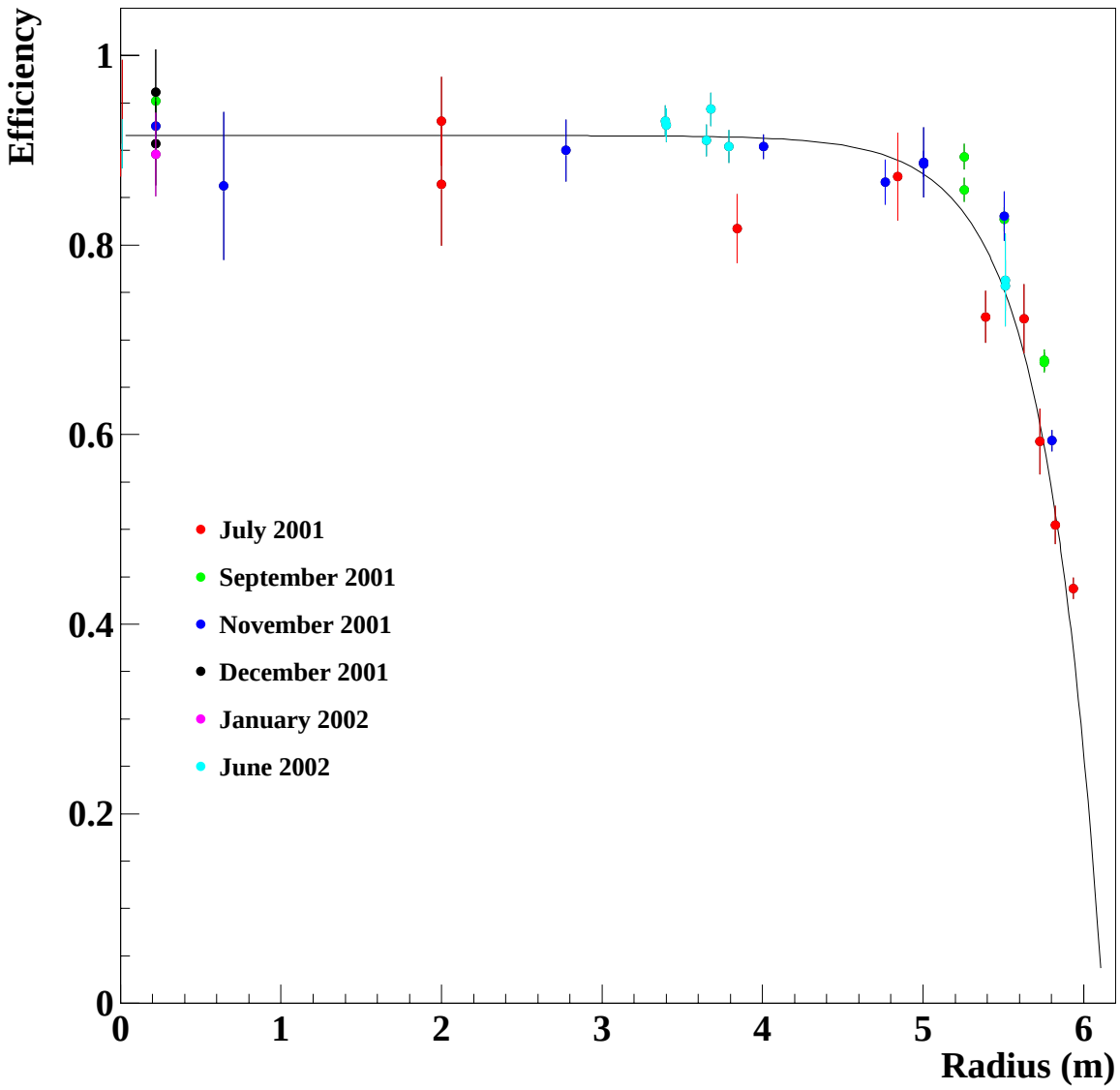

Figure C.2: Efficiency vs source radial position with 3.0 MeV energy threshold cut. Efficiency at center is $\epsilon_0 = 0.915 \pm 0.046$.

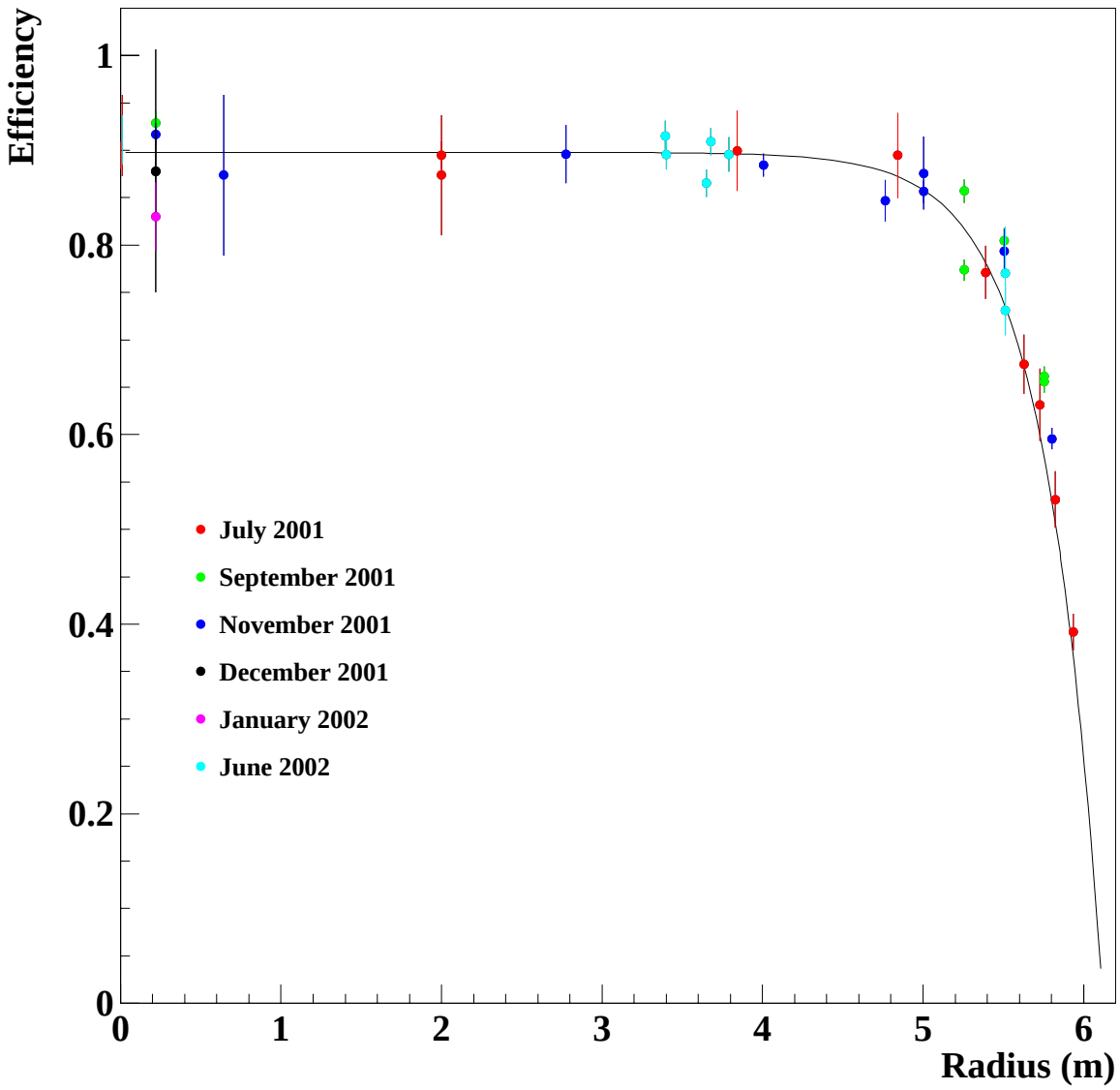

Figure C.3: Efficiency vs source radial position with 4.0 MeV energy threshold cut. Efficiency at center is $\epsilon_0 = 0.898 \pm 0.042$.

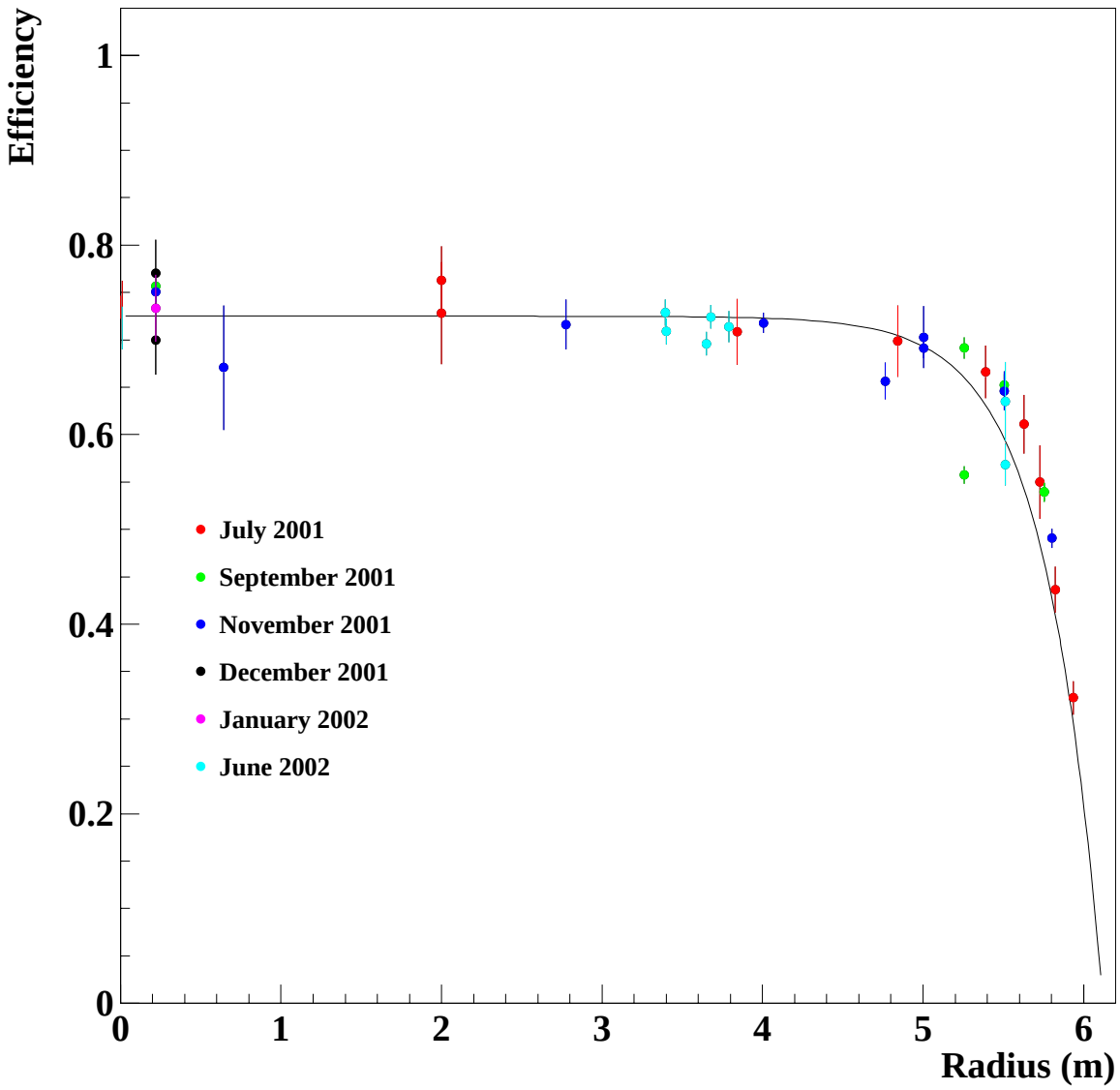

Figure C.4: Efficiency vs source radial position with 5.0 MeV energy threshold cut. Efficiency at center is $\epsilon_0 = 0.725 \pm 0.037$.

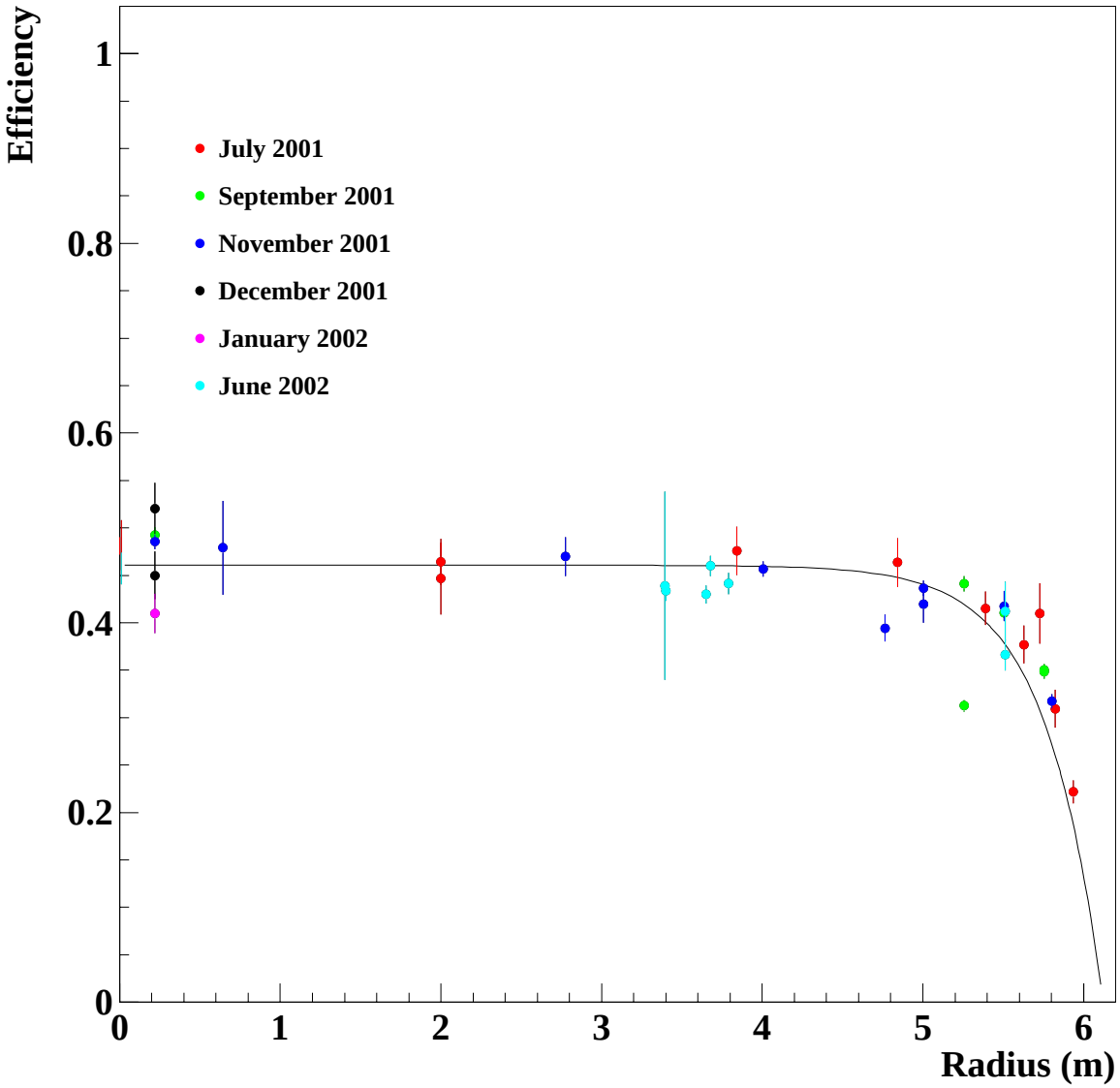

Figure C.5: Efficiency vs source radial position with 6.0 MeV energy threshold cut. Efficiency at center is $\epsilon_0 = 0.461 \pm 0.029$.

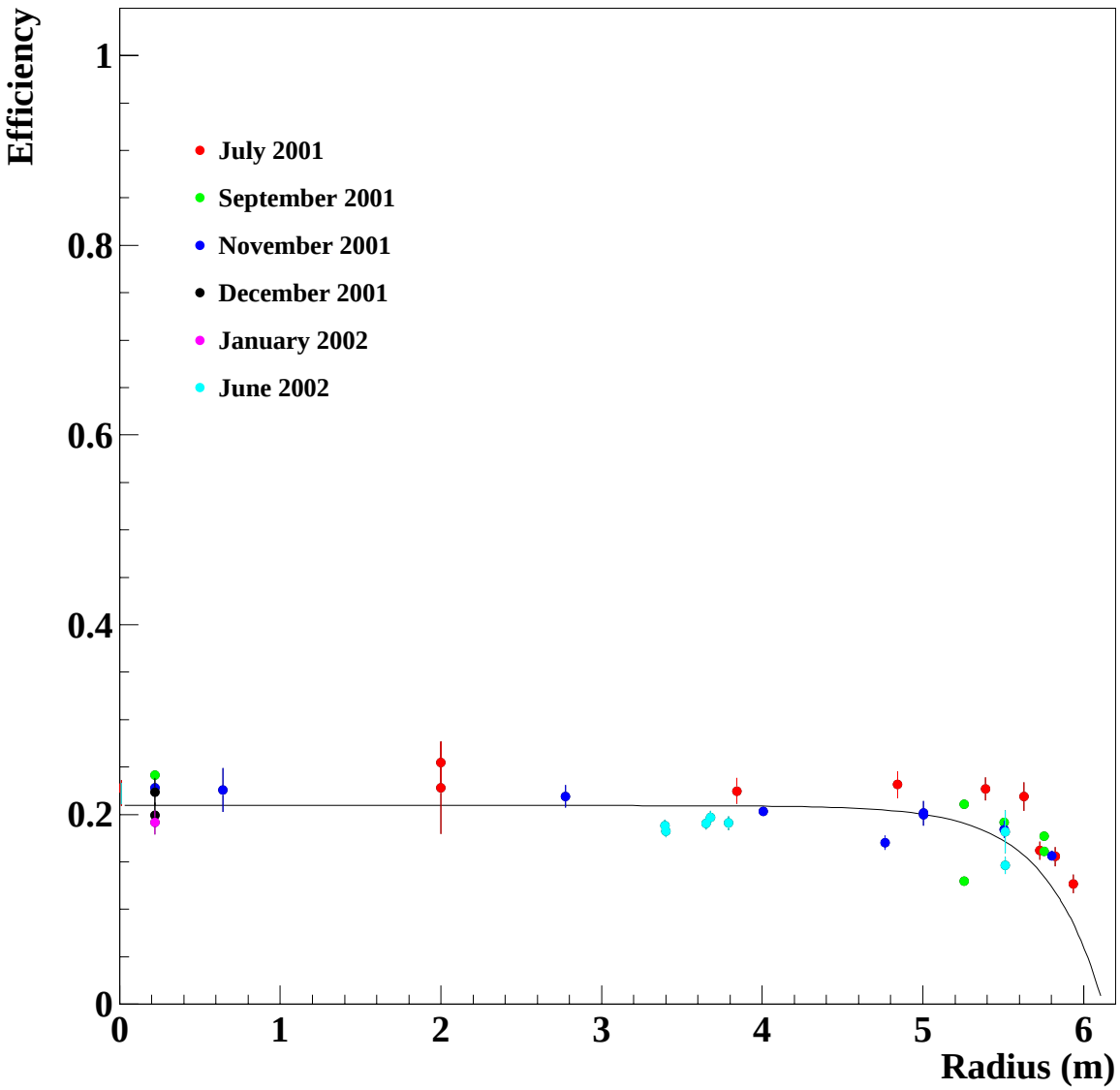

Figure C.6: Efficiency vs source radial position with 7.0 MeV energy threshold cut. Efficiency at center is $\epsilon_0 = 0.209 \pm 0.017$.